2010

Mesoporous metal oxide materials for catalysis and biotechnology applications

Enruo Guo
Iowa State University

Mesoporous metal oxide materials for catalysis and biotechnology applications

by

Enruo Guo

A thesis submitted to the graduate faculty

in partial fulfillment of the requirements for the degree of

MASTER OF SCIENCE

Major: Chemistry

Program of Study Committee:
Victor Shang-Yi Lin, Major Professor
Marek Pruski
Aaron Sadow

Iowa State University

Ames, Iowa

2010

TABLE OF CONTENTS

ACKNOWLEDGEMENT

I would like to express my gratitude to all these people who provide so much help during the three years.

I am deeply indebted to my advisor Professor Victor S. Y. Lin, whose help, stimulating suggestions and encouragement supported me in all the time of research and writing the thesis.

To my past and present POS committee members, Dr. Marek Pruski, Dr. Aaron Sadow, Dr. Emily Smith, and Dr. Zhiqun Lin, thanks for their time and guidance.

To Dr. Yulin Huang, thanks his guidance and knowledge in catalysis related projects, and his help in taking TEM images.

To Dr. James Anderegg, research scientist in Ames Laboratory, thanks his suggestions in ceria synthesis and efforts in XPS analysis.

To the staffs in hybridoma, SEM, EDS, TGA, ICP-MS facilities from Iowa State University, thanks for their help.

To scientists, postdoctoral and senior graduates in Prof. Lin's group, thanks their patience and kindness in helping me start the research and sharing their valuable experience.

To my dear parents, thanks their endless love and supports, without which I could not achieve the goal, and the priceless treasures I will seal forever.

To my husband, thanks his company and encouragement in the long journey, the share of laughs and tears.

To my friends, either in China or in US, thanks their friendship and selfless supports.

To U.S. Department of Energy, Ames laboratory, thanks the funding support to the projects.

ABSTRACT

The research presented here involves the application of mesoporous silica nanoparticles in heterogeneous catalysis and biomedical study.

Since the discovery of mesoporous silica nanoparticle (MSN), it has been studied as solid catalyst support. We studied the catalytic activity of CO hydrogenation and the selectivity to C_2 oxygenates by encapsulating monodispersed rhodium (Rh) nanoparticles during the synthesis of MSN in situ, and further modified by manganese oxide. The catalysts showed a higher reactivity in CO hydrogenation and a better selectivity to the desired product ethanol.

Structure directing agent plays a big role in mesophase structure, as well as affecting the distribution of functional group during the co-condensation. We developed an anionic surfactant (PME), by which we increased the interaction of the calcium site with the head group of surfactant, synthesizing a mesoporous calcium silicate material. The catalytic activity in transesterification reaction is better than the cationic surfactant (CTAB) templated material.

Also, previous studies in our group showed the potential of MSN, which were biocompatible as drug delivery vehicles. We exploited the biological application of MSN by chemically bonding ceria nanoparticles as the caps for stimuli responsive control release system. Furthermore, it showed pH dependent antioxidant properties when mixed with H_2O_2, and better endocytosis efficiency and protection to normal cells than naked ceria nanoparticles.

CHAPTER 1. GENERAL INTRODUCTION

Organization

This thesis is organized in five chapters. The first chapter is general introduction to MSN and its application in heterogeneous catalysis and biology. Chapter 2 and 3 are journal article. In Chapter 2, Yulin Huang is the primary author. My contribution is mainly on the reactivity test on CO hydrogenation of a series of catalysts, comparing the CO conversion and C_{2+} selectivity to those commercial available catalysts, catalysts by impregnation method, with our in-situ encapsulation synthesized MSNRhNPs. This work is prepared to submit to *Nano-Letters*. Chapter 3 is one section from an accepted paper by *Topics in Catalysis*. The paper is the result of collaborate work with 3 other researchers. In particular, I investigated the synthesis of anionic surfactant templated mesoporous calcium silicate and tested its catalytic performance in transesterification reaction, by using the surfactant developed by Chih-Hsiang Tsai. While, the calcium silicate synthesized under cationic surfactant and without surfactant was studied by Tse-Ming Hsin and Senniang Chen, which I didn't included in my thesis. Chapter 4 is about cerium oxide nanoparticle, its application in biotechnology. I am the primary author, while Yannan contributed to cell experiments and images taken. Chapter 5 finishes the thesis with general conclusions.

Overview of Mesoporous Silica Materials

Since the discovery of the first ordered mesoporous materials (IUPAC: 2 nm < particle diameter < 50 nm), known as the M41S-type of silica mesophases, by researchers in Mobil Research and Development Corporation in the early 1990s,[1] the field has been

extensively investigated. By changing the synthesis conditions, it is possible to alter the order of the material and therefore create new types of structures. The three most important are: MCM-41, which is hexagonal,[2] cubic MCM-48 [3] and lamellar MCM-50. [4]

MCM-41 is the most widely studied M41S material, which is also our interest in this thesis. MCM-41 has high surface areas of up to 1200 m^2/g and large pore volumes. The pores are unidirectional and pore size distributions are narrow (see Figure 1). They can be tailed to diameters between 1.5 and 20 nm, while, the thickness of pore walls is between 1 and 1.5 nm.[5] A typical X-ray diffraction pattern of MCM-41 shows the hexagonal symmetry of the pore ordering (space group: *p6m*), which contains four main reflection peaks (d_{100}, d_{110}, d_{200} and d_{210}), while no reflections can be observed at higher degrees because of the amorphous structure at atomic level.

A large diversity of synthetic approach is applied to synthesis of mesoporous silica materials. Basically, surfactant type, the specific synthesis mechanism and the interaction of the silica source with the template molecules determine the final material's meso-structure. For example, MCM-41 materials are made by a S^+I^- direct interaction between a positively charged surfactant and a negatively charged silica source in a basic condition.[5] A general synthetic route can be described as dissolution of template solution in a certain solvent, adjusting pH, temperature, and other additives, followed by addition of the silica source (tetraethyl orthosilicate, metasilicate, fumed silica etc.). Then stirring for a period at a certain temperature allows hydrolysis and condensation of the inorganic species. In next step, the products will be recovered, washed and dried. Finally, the template needs to be removed by calcinations or extraction methods.

The synthetic recipe of MCM-41 in our group was developed by our previous members based on reported literature.[6-8] In a typical synthesis, a silica source tetraethyl orthosilicate was added to an alkaline solution of CTAB (cetyl trimethyl ammonium bromide) as the surfactant at 353K with vigorous stirring. After stirring for 2 h, the suspension was filtered and washed by water and an organic solvent. To remove the surfactant, the as-made material either was calcined at 823 K or refluxed with hydrogen chloride in methanol at 333K.

The key parameters for the mesoporous material synthesis are the hydrogel composition, the type and length of the surfactant, the pH, the temperature and time. In particular, packing factor or g factor, describes the hydrophobic-hydrophilic balance between the alkyl chain and the head group, thus the tendency of the alkyl chain to minimize its contact with water and maximize its organic-interaction. [9]

The packing factor (g) can be expressed as $g = V/ a_0 l$, where V represents the total volume of the surfactant chains plus any additive between the chains; a_0 is the effective head group area and l is the kinetic surfactant tail length. As the value of g increases above a critical value, mesophase transitions occur (see Figure 2). When the polar head group has a large surface area, spherical structures are obtained. On the other hand, lamellar or rod packing occurs when the head groups are packed tightly with large aggregation numbers.

Functionalization and Application of Mesoporous Silica Materials

In order to take advantage of MCM-41 materials in the application of heterogeneous catalysis and drug delivery, we need to modify the surface of the material by functionalizing with metal ions or metallic nanoparticles or organic group. These functionalities either serve

as catalytically active sites, or as the linker to other nanoparticles or macromolecules, which later "cap" the pores of MCM-41.

Basically, there are two methods of functonaliztion: co-condensation and grafting. Co-condensation involves the *in-situ* condensation of the organosilane with TEOS, which results in a homogenous distribution of the organic group on the surface of the silica material; Grafting involves the post-synthesis of organosilane with the silanol group on the non-functional MCM-41 material at high temperature. Since it's a solid-liquid reaction, the functionalization is limited by the accessibility of the silanol group, and the distribution is not homogenous compared to the one-port co-condensation method. However, due to different applications, properties of the reactant and characterization requirement, we employed both of the methods in our following research.

One application of MCM-41 material is as the heterogeneous catalyst support, due to the relatively large pores, which facilitates mass transfer, and the very high surface area, which allows a high concentration of active sites per mass of material.

In order to modify the nature of the framework, it is vitally important to incorporate heteroatoms into the inert framework or walls of mesoporous materials. It is generally observed that the degree of metal incorporation as well as coordination of metal sites in the mesopore structure is dependent on the synthesis conditions, gel's pH, temperature, time and the nature of metal precursor used. [10]

Highly dispersed metal nanoparticles play a significant role in many catalytic reactions.[11] However, for high temperatures process, surface atoms are highly mobile, leading to the interparticle diffusion and, subsequent growth of metal particles to bulk size.[12] Thus, researchers use inert inorganic supports with rigid frameworks and high surface areas

to get higher dispersion of metal-nanoparticle catalysts. For the fabrication of monodisperse metal nanoparticles within the channels of mesoporous materials, conventional methods such as incipient wetness is evidently not a good choice, since metal nanoparticles with bimodal size distribution would be obtained on both internal and external surfaces of mesoporous channels. Selective encapsulation of monodisperse metal nanoparticles inside the channels of mesoporous silica is highly desirable. Currently, numerous strategies have been reported for the encapsulation of metal nanocomposites, which include: *in situ* encapsulation,[13,14] organometallic methodologies[15, 16] and surface functionalization schemes.[17]

In situ encapsulation method of monodisperse metal nanoparticles is typically based on pre-synthesis of nanoparticles with narrow size distribution (see Figure 3). Due to the higher stability of the pre-synthesized nanoparticles as compared to molecular metal clusters, such nanoparticles can be dispersed in the synthesis mixtures of mesoporous materials (generally, strong acidic or basic condition). Upon precipitation of the inorganic species, these metal nanoparticles are expected to be incorporated into the framework of mesoporous materials.[13] The metallic nanoparticles could keep their uniformity even after high temperature treatment, and show good catalytic activity, due to confinement of the silica materials. In early studies, Schuth et al. found the 2-nm Pt nanoparticles encapsulated in MCM-41 type materials showed very good performance in CO oxidation.[18] Johnson et al. found that monodispersed nanoclusters confined in MCM-41 materials had an improved enatioselectivity in hydrogenation reaction compared to the homogenous catalysts.[19] Fukuoka also reported that highly dispersed Pt nanoparticles in mesoporous FMS-16 materials were very effective for CO conversion.[20] All the above results indicate that confining of metallic-bimetallic nanoparticles in the mesoporous silica matrix is applicable and achievable, which

give us a hint to design a better catalyst for our following research: ethanol production from synthetic gas.

In our method, we introduced polyvinylpyrrolidone (PVP) as the stabilizer, and successfully synthesized 2nm-sized Rh nanoparticles (NPs) in solution environment. Later we applied the *in-situ* encapsulation method, to make the Rh NPs loaded on MCM-41 type material. Rh based materials were well known for their excellent performance in CO hydrogenation. Our catalysts showed not only higher reactivity than the previously reported Rh catalysts, but also better selectivity to the desired product ethanol. The reactivity of MSNRhNPs in CO hydrogenation and especially the selectivity to ethanol were further improved after it was modified by manganese oxide. We will discuss the details in the following chapter.

Previously, our group developed a new cooperative catalytic system comprised of a series of bifunctional mesoporous mixed oxide materials, which contain both Lewis acidic and basic sites for the synthesis of biodiesel from various free fatty acids (FFA)-containing oil feed stocks.[21] These materials were synthesized by cationic surfactant (CTAB) by introducing silicon precursor (TEOS) and calcium precursor (CaO) at the same time under basic condition in elevated temperature. Even though the mesoporous calcium silicate (MCS) showed the ability to catalyze both esterification and transesterification reaction with good recyclability, the catalytic efficiency is still need to be improved. By employing a new synthetic strategy, using anionic surfactant as structure directing agent instead of cationic surfactant, we are trying to increase the possibility of contact between the active site (calcium oxide) with the reactant.

Anionic surfactants that can self-assemble into micelles in water have been used as structure-directing templates for the synthesis of mesoporous silica materials.[22] Recently, a series of Anionic-surfactant-templated Mesoporous Silica (AMS) have been synthesized, by using 3-aminopropyltriethoxysilane (APS) as a co-structure directing agent (CSDA), which can interact with the anionic head group of the surfactant (SDA). Generally, the formation undergoes "$S^-N^+{\sim}I^-$" pathway (S^-: anionic surfactant, N^+: cationic amino group and I^-: inorganic species). Removal of the anionic surfactant by extraction led to the functionalized AMS containing amino groups on the silica surface.[23, 24-29]

According to Tatsumi et al.,[30] the amino groups derived from APS estimated by CHN elemental analysis and argentometric titration, were on the surfaces; however the MCM-41 type materials synthesized with a cationic surfactant by direct co-condensation had a random distribution of the amino groups, shown in Figure 3. Amino-functionalized AMS via the anionic surfactant templating route also showed a higher Co^{2+} cations adsorption capacity than amino-functionalized MCM-41. The difference of the amino functionality distribution inspires us to design a novel solid base catalyst in biodiesel production. In our study, positively charged calcium ions were introduced to interact with the phosphate groups of the anionic PME surfactant molecules. Under basic conditions, hydrolyzed TEOS easily coordinates with the calcium/surfactant in an $S^-M^+I^-$ (S^-: anionic surfactant, M^+: metal cation and I^-: inorganic species) complex system and forms ordered structure. After the removal of surfactants, the calcium sites would be exposed to the surface and react with methanol and feedstock effectively. We will further discuss the catalytic system in Chapter 3.

Among the variety of inorganic materials in biomedical applications, mesoporous silica nanoparticles have many attractive features, such as large surface area, high pore

volume, ordered pore structures, which can be used in storage and delivery of small molecules. After tuning the pore size, larger molecules such as protein can also be loaded.[31] [32] In the recent years, our group reported a series results in design of functional mesoporous silica materials for stimuli-responsive controlled-release delivery of pharmaceutical drugs, genes, and other chemicals.[32-42]

CdS nanoparticles were chemically linked on MSN surface via a cleavable disulfide bond, blocking the mesopores of MSN (see Figure 4), which prevented the leaching of the loaded guest molecules.[33] The release of guest molecules was triggered by exposing the capped MSNs to chemical stimulation that could cleave the disulfide linker, and thus remove the nanoparticle caps and release the pore-entrapped guest molecules.

Cerium oxide nanoparticles have attracted attention in biomedical application recently.[43-48] Surface oxygen vacancies, the intrinsic property of cerium oxide, allows it to have two oxidation state: +3 and +4, and can flip-flop between the two during redox reaction.[49] It has been reported that ceria nanoparticles could inhibit the increase in the intracellular concentration of reactive oxygen intermediates of rat retina cell, prevent photoreceptor cell from light-induced degeneration in vivo,[44] and even mimic the catalytic activity of superoxide dismutase.[50] As reported, these activities directly correlate with the ratio of Ce (+3) to Ce (+4). A higher concentration of Ce (+3) would result in a better activity in superoxide scavenging process.[46] According to the literature, when particle size decreased, it would result in an increase in surface area to volume ratio, giving rise to a larger surface oxygen vacancy.[51] Experiment shows that ceria with particle size around 5 nm is able to regenerate and acts as catalysts.[44] At the same time, other researchers found cytotoxicity and oxidative stress induced by cerium oxide with larger size (such as 20 nm) in cultured BEAS-

2B cells [52] and human lung cancer cells.[53] Interestingly, researchers also found a selective protection of nanoceria to normal cells when treated with radiation or H_2O_2, but not to tumor cells[43, 47], as shown in Figure 7. The different protection may come from the intra- and extracellular pH differences presented in normal versus tumors tissue due to metabolic activity.

In order to overcome CdS nanoparticle induced cytotoxicity, as well as applying a new function to the release system, we studied ceria nanoparticles (CNPs) as the mesopore caps acting as an antioxidant to scavenge reactive oxygen species induced by toxic drug. This work will be included in Chapter 5.

The functionalized mesoporous silica materials developed in our lab have been demonstrated for a variety of applications in drug controlled-release, catalysis and biomedicine. In order to fully take advantage of the unique properties of MSN, further investigation is highly demanded, such as tuning of pore size and surface functionalization. It is of our interest for further applications: a smart vehicle, selectively absorbing valuable components from economically-based algae.

References

1. Kresge, C. T.; Leonowicz, M. E.; Roth, W. J.; Vartuli, J. C.; Beck, J. S., *Nature (London, U. K.)* **1992,** *359* (6397), 710-12.

2. Beck, J. S.; Vartuli, J. C.; Roth, W. J.; Leonowicz, M. E.; Kresge, C. T.; Schmitt, K. D.; Chu, C. T. W.; Olson, D. H.; Sheppard, E. W.; et al., *J. Am. Chem. Soc.* **1992,** *114* (27), 10834-43.

3. McCullen, S. B.; Vartuli, J. C.; Kresge, C. T.; Roth, W. J.; Beck, J. S.; Schmitt, K. D.; Leonowicz, M. E.; Schlenker, J. L.; Shih, S. S.; Lutner, J. D., *Access Nanoporous Mater., [Proc. Symp.]* **1995**, 1-11.

4. Huo, Q.; Margolese, D. I.; Stucky, G. D., *Chem. Mater.* **1996,** *8* (5), 1147-60.

5. Selvam, P.; Bhatia, S. K.; Sonwane, C. G., *Industrial & Engineering Chemistry Research* **2001,** *40* (15), 3237-3261.

6. Cai, Q.; Luo, Z.-S.; Pang, W.-Q.; Fan, Y.-W.; Chen, X.-H.; Cui, F.-Z., *Chem. Mater.* **2001,** *13* (2), 258-263.

7. Huh, S.; Wiench, J. W.; Yoo, J.-C.; Pruski, M.; Lin, V. S. Y., *Chem. Mater.* **2003,** *15* (22), 4247-4256.

8. Huh, S.; Chen, H.-T.; Wiench, J. W.; Pruski, M.; Lin, V. S. Y., *Angew. Chem., Int. Ed.* **2005,** *44* (12), 1826-1830.

9. Ciesla, U.; Schuth, F., *Microporous Mesoporous Mater.* **1999,** *27* (2-3), 131-149.

10. Meynen, V.; Cool, P.; Vansant, E. F., *Microporous Mesoporous Mater.* **2009,** *125* (3), 170-223.

11. Janicke, M.; Kumar, D.; Stucky, G. D.; Chmelka, B. F., *Stud. Surf. Sci. Catal.* **1994,** *84* (Zeolites and Related Microporous Materials, Pt. A), 243-50.

12. Bell, A. T., *Science* **2003,** *299* (5613), 1688-1691.

13. Moulijn, J. A.; van Diepen, A. E.; Kapteijn, F., *Appl. Catal., A* **2001,** *212* (1-2), 3-16.

14. Zhu, J.; Konya, Z.; Puntes, V. F.; Kiricsi, I.; Miao, C. X.; Ager, J. W.; Alivisatos, A. P.; Somorjai, G. A., *Langmuir* **2003,** *19* (10), 4396-4401.

15. Aprile, C.; Abad, A.; Garcia, H.; Corma, A., *J. Mater. Chem.* **2005,** *15* (41), 4408-4413.

16. Agger, J. R.; Anderson, M. W.; Pemble, M. E.; Terasaki, O.; Nozue, Y., *J. Phys. Chem. B* **1998,** *102* (18), 3345-3353.

17. Kim, S.-W.; Son, S. U.; Lee, S. I.; Hyeon, T.; Chung, Y. K., *J. Am. Chem. Soc.* **2000,** *122* (7), 1550-1551.

18. Guari, Y.; Thieuleux, C.; Mehdi, A.; Reye, C.; Corriu, R. J. P.; Gomez-Gallardo, S.; Philippot, K.; Chaudret, B.; Dutartre, R., *Chem. Commun. (Cambridge, U. K.)* **2001,** (15), 1374-1375.

19. Junges, U.; Jacobs, W.; Voigt-Martin, I.; Krutzsch, B.; Schueth, F., *J. Chem. Soc., Chem. Commun.* **1995,** (22), 2283-4.

20. Johnson, B. F. G., *Top. Catal.* **2003,** *24* (1-4), 147-159.

21. Fukuoka, A.; Kimura, J.-I.; Oshio, T.; Sakamoto, Y.; Ichikawa, M., *J. Am. Chem. Soc.* **2007,** *129* (33), 10120-10125.

22. Sun, J.; Ma, D.; Zhang, H.; Liu, X.; Han, X.; Bao, X.; Weinberg, G.; Pfaender, N.; Su, D., *J. Am. Chem. Soc.* **2006,** *128* (49), 15756-15764.

23. Lin, V. S.-Y.; Nieweg, J. A.; Verkade, J. G.; Reddy, C. R. V.; Kern, C. Mesoporous silicate-alkaline earth oxide composite catalysts for manufacture of biodiesel from fats and glycerides. 2008021232,2008.

24. Huo, Q.; Margolese, D. I.; Ciesla, U.; Feng, P.; Gier, T. E.; Sieger, P.; Leon, R.; Petroff, P. M.; Schueth, F.; Stucky, G. D., *Nature (London, U. K.)* **1994,** *368* (6469), 317-21.

25. Garcia-Bennett, A. E.; Kupferschmidt, N.; Sakamoto, Y.; Che, S.; Terasaki, O., *Angew. Chem., Int. Ed.* **2005,** *44* (33), 5317-5322.

26. Garcia-Bennett, A. E.; Miyasaka, K.; Terasaki, O.; Che, S., *Chem. Mater.* **2004,** *16* (19), 3597-3605.

27. Che, S.; Li, H.; Lim, S.; Sakamoto, Y.; Terasaki, O.; Tatsumi, T., *Chem. Mater.* **2005,** *17* (16), 4103-4113.

28. Garcia-Bennett Alfonso, E.; Kupferschmidt, N.; Sakamoto, Y.; Che, S.; Terasaki, O., *Angew Chem Int Ed Engl* **2005,** *44* (33), 5317-22.

29. Gao, C.; Qiu, H.; Zeng, W.; Sakamoto, Y.; Terasaki, O.; Sakamoto, K.; Chen, Q.; Che, S., *Chem. Mater.* **2006,** *18* (16), 3904-3914.

30. Gao, C.; Sakamoto, Y.; Sakamoto, K.; Terasaki, O.; Che, S., *Angew. Chem., Int. Ed.* **2006,** *45* (26), 4295-4298.

31. Gao, C.; Sakamoto, Y.; Terasaki, O.; Che, S., *Chem.--Eur. J.* **2008,** *14* (36), 11423-11428.

32. Yokoi, T.; Yoshitake, H.; Yamada, T.; Kubota, Y.; Tatsumi, T., *J. Mater. Chem.* **2006,** *16* (12), 1125-1135.

33. Han, Y.-J.; Stucky, G. D.; Butler, A., *J. Am. Chem. Soc.* **1999,** *121* (42), 9897-9898.

34. Slowing, II; Trewyn, B. G.; Lin, V. S. Y., *J. Am. Chem. Soc.* **2007,** *129* (28), 8845-8849.

35. Lai, C. Y.; Trewyn, B. G.; Jeftinija, D. M.; Jeftinija, K.; Xu, S.; Jeftinija, S.; Lin, V. S. Y., *J. Am. Chem. Soc.* **2003,** *125* (15), 4451-4459.

36. Radu, D. R.; Lai, C. Y.; Jeftinija, K.; Rowe, E. W.; Jeftinija, S.; Lin, V. S. Y., *J. Am. Chem. Soc.* **2004,** *126* (41), 13216-13217.

37. Trewyn, B. G.; Whitman, C. M.; Lin, V. S. Y., *Nano Lett.* **2004,** *4* (11), 2139-2143.

38. Giri, S.; Trewyn, B. G.; Stellmaker, M. P.; Lin, V. S. Y., *Angewandte Chemie-International Edition* **2005,** *44* (32), 5038-5044.

39. Slowing, II; Trewyn, B. G.; Giri, S.; Lin, V. S. Y., *Adv. Funct. Mater.* **2007,** *17* (8), 1225-1236.

40. Torney, F.; Trewyn, B. G.; Lin, V. S. Y.; Wang, K., *Nat. Nanotechnol.* **2007,** *2* (5), 295-300.

41. Trewyn, B. G.; Giri, S.; Slowing, II; Lin, V. S. Y., *Chemical Communications* **2007,** (31), 3236-3245.

42. Zhao, Y.; Trewyn, B. G.; Slowing, I. I.; Lin, V. S. Y., *J. Am. Chem. Soc.* **2009,** *131* (24), 8398-8400.

43. Mortera, R.; Vivero-Escoto, J.; Slowing, I. I.; Garrone, E.; Onida, B.; Lin, V. S. Y., *Chem. Commun. (Cambridge, U. K.)* **2009,** (22), 3219-3221.

44. Vivero-Escoto, J. L.; Slowing, I. I.; Wu, C.-W.; Lin, V. S. Y., *J. Am. Chem. Soc.* **2009,** *131* (10), 3462-3463.

45. Tarnuzzer, R. W.; Colon, J.; Patil, S.; Seal, S., *Nano Lett.* **2005,** *5* (12), 2573-2577.

46. Chen, J.; Patil, S.; Seal, S.; McGinnis, J. F., *Nat. Nanotechnol.* **2006,** *1* (2), 142-150.

47. Schubert, D.; Dargusch, R.; Raitano, J.; Chan, S.-W., *Biochem. Biophys. Res. Commun.* **2006,** *342* (1), 86-91.

48. Heckert, E. G.; Karakoti, A. S.; Seal, S.; Self, W. T., *Biomaterials* **2008,** *29* (18), 2705-2709.

49. Perez, J. M.; Asati, A.; Nath, S.; Kaittanis, C., *Small* **2008,** *4* (5), 552-556.

50. Karakoti, A. S.; Singh, S.; Kumar, A.; Malinska, M.; Kuchibhatla, S. V. N. T.; Wozniak, K.; Self, W. T.; Seal, S., *J. Am. Chem. Soc.* **2009,** *131* (40), 14144-14145.

51. Esch, F.; Fabris, S.; Zhou, L.; Montini, T.; Africh, C.; Fornasiero, P.; Comelli, G.; Rosei, R., *Science* **2005,** *309* (5735), 752-755.

52. Korsvik, C.; Patil, S.; Seal, S.; Self, W. T., *Chem. Commun. (Cambridge, U. K.)* **2007,** (10), 1056-1058.

53. Deshpande, S.; Patil, S.; Kuchibhatla, S. V. N. T.; Seal, S., *Appl. Phys. Lett.* **2005,** *87* (13), 133113/1-133113/3.

54. Park, E.-J.; Choi, J.; Park, Y.-K.; Park, K., *Toxicology* **2008,** *245* (1-2), 90-100.

55. Lin, W.; Huang, Y.-w.; Zhou, X.-D.; Ma, Y., *Int. J. Toxicol.* **2006,** *25* (6), 451-457.

Tables and Figures

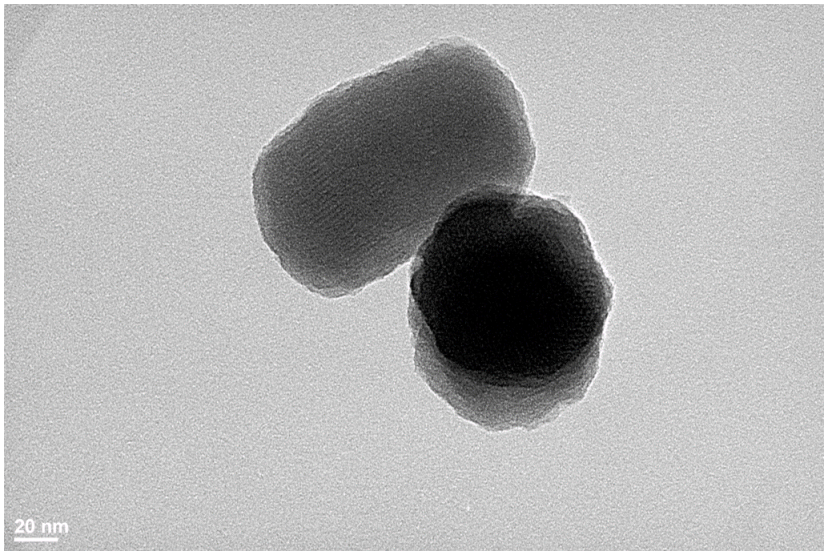

Figure 1. TEM image of the honeycomb structure of MCM-41.

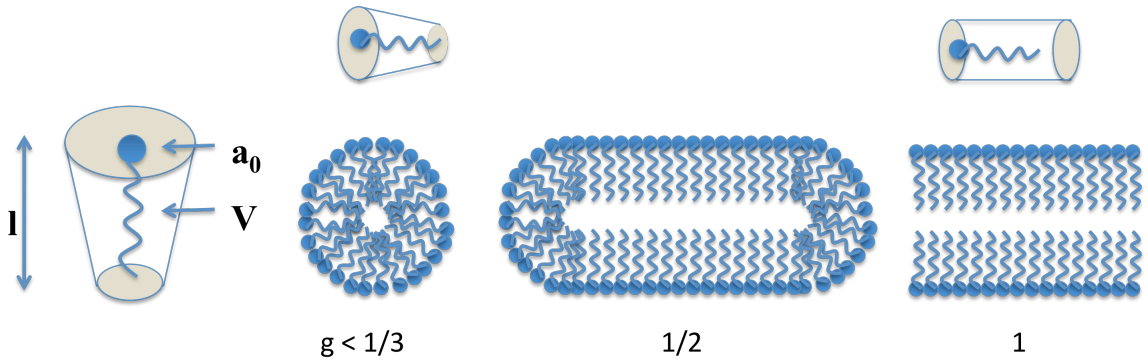

Figure 2. Schematic representation of values of g factor.[10]

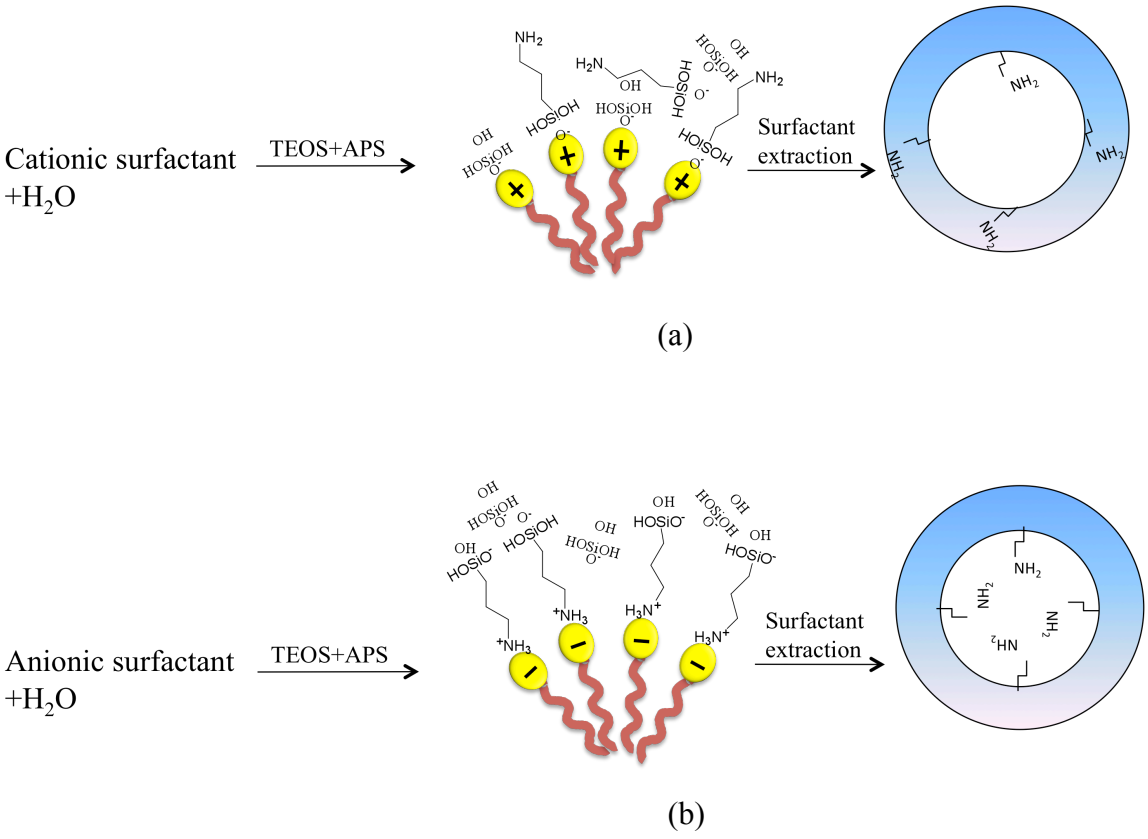

Figure 3. Illustration of the location of the aminopropyl group in amino-functionalized mesoporous silica synthesized via (a) the cationic templating and (b) the anionic templating routes.[32]

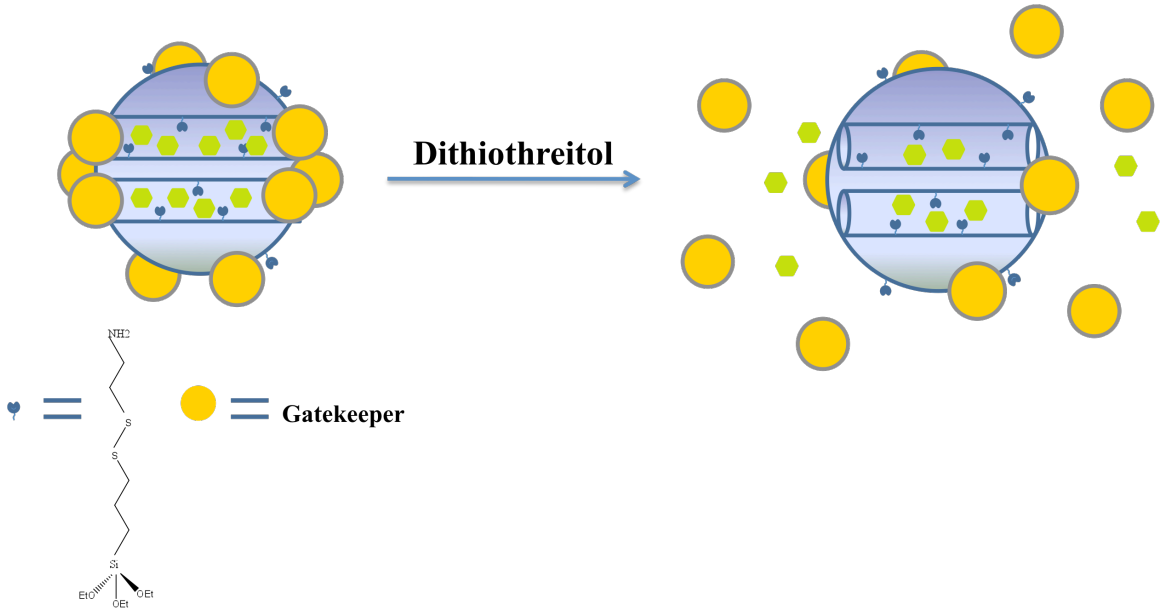

Figure 4. Schematic representation of the solid nanoparticle-capped MSN based drug/neurotransmitter delivery system. The controlled release mechanism of the system is based on chemical reduction of the disulfide linkage between the caps and MSN.[35]

CHAPTER 2. MN-MODIFIED AND WELL-DEFINED RH NANOPARTICLES SUPPORTED ON MESOPOROUS SILICA NANOPARTICLES: HIGHLY-SELECTIVE SYNTHESIS OF ETHANOL FROM SYNGAS

A paper to be submitted to *Nano Letters*

Yulin Huang,[1] Weihua Deng,[2] Enruo Guo,[1] Senniang Chen,[1] Po-Wen Chung,[1] Brian G. Trewyn,[1] Victor S.-Y. Lin[1,*]

1. Department of Chemistry and Ames Laboratary-U.S. Department of Energy, Iowa State University, Ames, IA 50011, 2. Center for Sustainable Environmental Technologies, Iowa State University, Ames, IA 50011

**Corresponding author.*

Abstract

Well-defined and monodispersed rhodium (Rh) nanoparticles as small as ~2 nm were synthesized with polyvinylpyrrolidone (PVP) polymer in ethanol. And the as-made PVP-stabilized Rh nanoparticles were dispersed and encapsulated in mesoporous silica nanoparticles *in situ* during the synthesis of this high-surface-area mesoporous silica nanoparticle (MSN) support. Catalytic performance of the MSN-supported Rh nanoparticles (MSNRhNPs) was modified by manganese oxides and studied with CO hydrogenation. MSNRhNPs were active for the CO hydrogenation and the selectivity to C2 oxygenates reached the highest point without formation of by-product methanol after the Rh nanoparticles were modified by manganese oxide during the formation of MSN.

Introduction

It is well known that higher alcohols synthesized from natural gas, coal, or biomass can be used as a renewable energy alternative, such as additives to gasoline and an easily transportable source of hydrogen.[1-4] Because ethanol could not only decrease the dependence on imported cruel oil but also would have a positive environmental impact, synthesis of ethanol selectively from syngas (CO and H_2), which can be made from coal or biomass pyrolysis, has been a topic of growing interesting from both industrial and academic points of views. In the catalytic synthesis of ethanol since the 1980s,[5] rhodium-based catalysts have been known for decades to be the most selective catalysts for the synthesis of C_{2+} oxygenates, including ethanol, acetaldehyde and acetic acid, due to the unique CO adsorption behavior on Rh surface,[6,7] although some other transition metal catalysts were reported.[2,8-15] Most of the attention on Rh-based catalysts for ethanol synthesis from syngas was and is still on the influences of catalyst precursors,[16-21] supports[6,22-28] and promoters or additives[16,21,22,24,29-43] on the activity and selectivity. And most of these Rh-based heterogeneous catalysts were made from impregnation of rhodium salt solution which then was followed by calcinations of the as-made solid at high temperature and reduction of rhodium oxides to metallic rhodium particles by hydrogen gas.[44-46] Usually rhodium particles from this process, including impregnation, calcination and reduction, have a very broad size distribution and vary a lot from batch to batch, because the control of particle size distribution especially on support surface is still very challenging especially at the required high temperature.[13] And that might be the reason there are only few studies on the size controlling of Rh particles in CO hydrogenation.[47] But, for CO hydrogenation or any other reactions catalyzed by immobilized Rh catalysts, Rh particle size controlling should be a very

important to adjust the percentage of surface metal atoms that are the only accessible to the reactants.[48,49] Therefore downsizing Rh particles, especially to nanometer scale, should be an efficient strategy to increase the reactivity and probably improve the selectivity, due to the dramatically increased percentage of surface metal atoms.

For downsizing metal catalyst particle, colloidal chemistry could be adopted to synthesize mono-dispersed metal nanoparticle with well-defined particle size in solution. After metal nanoparticle was made in colloidal solution, nanoparticle's dispersion on porous supports by impregnation is required. Mesoporous silica structures have been regarded as ideal catalyst supports due to their high surface area, tunable pore size and highly ordered alignment since its discovery at the beginning of 1990s.[27,50-52] However, in this methods, in a addition to the difficulty of controlling the homogeneous distribution of metal particles on porous supports surface, rhodium particle growing is still challenging for both chemists and chemical engineer, due to 1) the weak interaction (or physical adsorption) between metal nanoparticle and support surface and 2) the inevitable growth or sintering of catalyst particles.

Here we reported the successful synthesis of ~2.0 nm Rh particles (RhNPs) in alcoholic solution using a polymer, polyvinylpyrrolidone (PVP), as a nanoparticle stabilizer and subsequent encapsulate the as-made RhNPs in the framework of mesoporous silica nanoparticle (MSN) during *in situ* of the forming of MSN (Scheme 2-1). Comparing with commonly used MSN-supported Rh catalyst from incipient wetness impregnation of aqueous $RhCl_3$ solution (MSNRh), RhNPs encapsulated in MSN framework (MSNRhNPs) not only have a higher reactivity in CO hydrogenation but also have better selectivity to the desired

product ethanol. The reactivity of MSNRhNPs in CO hydrogenation and especially the selectivity to ethanol were further improved after it was modified by manganese oxide.

Allen, B. S. (1984), Bruner, J. (1960) and Cox, S. R. (1974) did the initial work in this area. But in Bruner's work [Bruner, J. (1960)] the definitive model is seen.

Results and Discussions

Synthesis of PVP-stabilized Rh Nanoparticles and Mesoporous Silica Nanoparticle Framework Encapsulated Rh Nanoparticles. Metal nanoparticles less than 10 nm that were well defined and monodispersed with controlled shape have been synthesized by colloid chemistry in recent years.[53-55] For the synthesis of Rh nanoparticles less than 2.0 nm, there are a few reported methods.[48,49,56,57] Because PVP is a water soluble polymer, PVP stabilized rhodium nanoparticles can be dispersed homogeneously in water which can be homogeneously distributed in aqueous solution for MSN synthesis. PVP-stabilized RhNPs were synthesized as reported with minor modifications.[48,49] PVP (Typical M_w = 29,000) was purchased from Sigma-Aldrich as the nanoparticle stabilizer. A 7.9 mmol/L PVP solution was prepared by dissolving the polymer into anhydrate ethanol. The PVP ethanolic solution was mixed with 7.1 mmol/L aqueous $RhCl_3$ (Rh, 38-40% from Strem Chemicals, Inc.) solution at room temperature, where the mole ratio between PVP and Rh^{3+} was 10.0. After reduction of rhodium in ethanol, solvent was evaporated by rotavap at 40 ^oC and the as-made Rh nanoparticles (RhNPs) were characterized by transmission electronic miscroscopy (TEM). TEM image (Figure 2-1a) shows that the Rh particles are well-defined and mono-dispersed spheres with ~2.0 nm in diameter and HRTEM image (Figure 2-1b)

combining with diffraction pattern indicates that these tiny RhNPs have the crystalline structures.

The as-made RhNPs (480.0 mg, including 40.0 mg Rh) were re-dissolved into water (10.0 mL, 0.6 mol) and mixed with water (470 mL, 26.1 mol), cetyltrimethylammonium bromide (CTAB, 2.0 g, 5.5 mmol), NaOH (7.0 mL x 2.0 mol/L, 14.0 mmol) at room temperature prior to the hydrolysis of tetraethoxyl orthosilicate (TEOS, 10.0 mL, 44.8 mmol) at 80 ^{o}C for 2.0 hours. After the hydrolysis, the grey solid was filtrated and dried under vacuum overnight. The catalytic material MSNRhNPs was made and ready for catalyst characterization, analysis and catalytic tests after the removal of template CTAB and PVP at 350 ^{o}C in air for 5 hours. Before reaction, MSNRhNPs was reduced in continuous H_2 flow (10 mL/min) at 310 ^{o}C with 450 psi pressure for at least 2 h. N_2 adsorption and desorption isotherms show that MSNRhNPs still had a typical mesoporous structure of MSN with a narrow pore size distribution as diameter was around 2.4 nm, surface area at 947 m^2/g and pore volume at 1.0 mL. X-ray powder diffraction indicated that MSNRhNPs were still full of highly ordered parallel channels, which could be seen clearly from Transmission Electron Microscopy (TEM) images (Figure 2-2a). In TEM image, a lot of tiny black spots could be seen in addition to the highly ordered parallel channels and these were RhNPs, which was further confirmed by Scanning Transmission Electron Microscopy (STEM) image in Figure 2-2b. From STEM images of MSNRhNPs, it is clear that 1) RhNPs were well-distributed over the mesoporous silica nanoparticle and 2) the supported RhNPs was almost the same size, around 2.0 nm in diameter, as unsupported RhNPs (as shown in Figure 2-1), although it is very difficult to accurately measure the size of small nanoparticles on mesoporous supports because TEM images taken from nanoparticles supported on mesoporous supports often

suffer from low contrast due to the decrease of the supporting material's electron transparency, and this behavior is magnified as particle size decreases, and nanoparticles on mesoporous silica are also in different focal planes during TEM imaging. Energy Dispersive X-ray (EDX) was used to determine the loading of Rh on MSNRhNPs and 1.6 wt% of Rh in this material was obtained basing on the atomic ratio between Si and Rh.

Synthesis of Rh-MSN and Mn^{n+} Modified Rh Catalysts through Impregnation Methods. MSNRhNPs' counterparts, Rh-MSN with 1.6 wt% of Rh loading, from traditional incipient wet-chemistry, impregnation methods, were synthesized (see supporting information) in order to compare their catalytic properties in CO hydrogenation reactions. For Rh catalysts in CO hydrogenation, many promoters were used to improve selectivity to C_2 (including ethanol and acetaldehyde) or C_{2+} oxygenates,[2-4] and among these reported promoters, Mn_xO_y was a very good candidate.[34-36,58,59] (Here, the oxidation states of Mn species usually could not be accurate and it will be addressed in the flowing studies in this paper.) Therefore, in order to improve the selectivities of MSNRhNPs and Rh-MSN to C_2 oxygnates, Mn^{n+} modified MSNRhNPs (MSNRhNPs-Mn) and Mn^{n+} modified Rh-MSN (Rh-Mn-MSN) were both synthesized by impregnation methods using $Mn(NO_3)_2$.

Modification of RhNPs by Mn^{n+} during *in situ* formation of MSN. It's a well-known challenge to control the distribution of metal ions on solid surface. Therefore, many catalysts, even with the same chemical composition, have different catalytic performances if they are from different companies or different research groups. For the bimetallic or multimetallic catalysts, the situation was even worse due to the difficulty to adjust the interaction between these different metals. In catalyst MSNRhNPs, RhNPs were distributed homogeneously in MSN particles as we can see from Figure 2-2. However, during the Mn^{n+}

modification procedure, the distribution of Mn^{n+} and the interaction between RhNPs and Mn^{n+} are still out of control due to the innate disadvantage of impregnation method. In order to achieve a homogeneous distribution of Mn^{n+} around RhNPs and the interaction between RhNPs and Mn^{n+}, we, for the first time, modify RhNPs by Mn^{n+} right during the formation of MSN as shown in Figure 1-2.

Typically, the as-made RhNPs (480.0 mg, including 40.0 mg Rh) were re-dissolved into water (10.0 mL, 0.6 mol) and mixed with water (470 mL, 26.1 mol), CTAB (2.0 g, 5.5 mmol), NaOH (7.0 mL x 2.0 mol/L, 14.0 mmol) at room temperature prior to the adding of $Mn(NO_3)_2 \cdot xH_2O$ (104.7mg, including 20.0 mg Mn) and the hydrolysis of TEOS (10.0 mL, 44.8 mmol) at 80 ^oC for 2.0 hours. After the hydrolysis of TEOS, the black solid was filtrated and dried under vacuum overnight. The catalytic material MSNRhNPsMn was made and ready for the catalyst characterization after the calcination at 350 ^oC in air for 5 hours. Before reaction, MSNRhNPsMn was also reduced in continuous H_2 flow as other catalysts. N_2 adsorption and desorption isotherms, XRD show that MSNRhNPsMn still has the typical highly ordered MSN parallel channel structure with high surface area (S_{BET} = 878 m^2/g), very narrow pore size distribution (d_{BJH} = 2.5 nm). TEM and STEM images (Figure 2-2) of MSNRhNPsMn show that RhNPs are distributed homogeneously through the whole structure of MSN and the particle size is still around 2.0 nm without change after modification with Mn^{n+}. EDX was used to determine the loading of Rh and Mn on MSNRhNPsMn and 1.6 wt% of Rh and 0.8 wt% of Mn in this material were found, which makes the ratio between Rh and Mn around 2.0.

X-ray Photoelectron Spectroscopy (XPS) Study. XPS was used to characterize the oxidation states of Rh and Mn in our catalysts on a Perkin-Elmer PHI 5500 XPS

spectrometer with a position-sensitive detector, a hemispherical energy analyzer in an ion-pumped chamber (evacuated to 2 x 10^{-9} Torr), and a Al Kα (BE = 1486.6 eV) X-ray source at 300 W with 15 kV acceleration voltage. For all of our experiments, the binding energy of silicon was forced to be 104.5 eV which was used as an internal standard for other elements' binding energy. Figure 3 shows the XPS results of RhNPs and MSNRhNPs. Before calcination (Figure 3a and 3b), the Rh $3d_{5/2}$ peak (~308 eV) could be fit by two peaks with bonding energies of 307.3 eV and 308.9 eV, corresponding to the metallic Rh (0) and the oxidized Rh (+3) respectively. As shown in Figure 2-3a, RhNPs was very stable in air at room temperature with 88 % of metallic Rh(0) and 12 % of oxidized Rh(+3). After being encapsulated in MSN, there is still 30 % of metallic Rh(0) as shown in Figure 2-3b. After calcinations in air at 350 ^{o}C for 5 h, from XPS spectroscopy, Si, Mn, Rh and O are the only four detectable elements in all of our catalysts reported here, which indicates that template CTAB and PVP were removed completely from MSNRhNPs surface. With calcination, Rh was oxidized almost completely to Rh_2O_3 (Figure 3c), which can be reduced back to metallic Rh(0) by H_2 easily during the reaction(Figure 2-3d). So the XPS data might indicate that all of Rh atoms in RhNPs could be accessible to at least O_2 and H_2 and might be accessible to CO as well under our reaction conditions. In any XPS spectroscopy of Mn^{n+} modified catalysts, Mn^{n+} was found. However, the oxidation states of Mn species could not be solved because of its lower intensity and the relatively small difference between binding energies of Mn^{2+}, Mn^{3+} and Mn^{4+}, which decreases the reliability of fitting theoretically. Therefore, it is better to use Mn^{n+} instead of other Mn species with defined oxidation states here.

Carbon Monoxide hydrogenation Catalyzed by Rh Catalysts. Here a laboratory scale flow and tubular reactor was used for the CO hydrogenation with low surface area SiC

as catalyst diluting reagent. Temperature was controlled by a Parr controller (4843) and two type-K thermocouples. Gas flows (CO and H_2 were all from Praxair and UHP) were regulated by two calibrated mass flow system (Parr mass flow system with Brooks mass flow controllers). Before syngas was charged to the reactor, catalyst was reduced with 10 mL/min H_2 flow at 450 psi and 632 K for two hours. Deionized water was charged into the condenser in order to dissolve most of alcohols from the reaction. Tail gas right after the tubular reactor from the reaction was analyzed on an on-line GC (Varian 3900 with CP-Molsieve 5A (10 m x 0.32 mm x 10 μm) and CP-PoraBOND Q (50 m x 0.53 mm x 10 μm)), and a thermal conductivity detector (TCD)) with 5 wt% Ar as an internal reference gas. Liquid samples were analyzed on another Varian 3900GC but with flame ionization detector (FID) and a CP-PoraBOND Q (50 m x 0.32 mm x 5 μm) column.

We found that MSN encapsulated RhNPs catalysts (MSNRhNPs) has higher activity (CO conversion) and better selectivity to C_2 oxygenates than that of Rh-MSN made from impregnation methods in CO hydrogenation (Entry 1 and 2 in Table 1). And these trends were kept very well at different reaction temperatures. Since catalytic activity comparison was based on assuming 100% dispersion for every catalyst, the difference of reactivity was most likely due to the difference between Rh particles sizes. After reaction at 573 K for 24 h, TEM images showed that the Rh particles on Rh-MSN (Figure 4a) from impregnation methods grew much faster and had a much broader particle distribution (Most of them were larger than 5.0 nm and some of them even were around 20 nm in diameter) compared to that of MSNRhNPs (Figure 4b) where most of RhNPs were still less than 5 nm in diameter. The larger Rh particle in Rh-MSN made CO and H_2 accessible surface Rh atoms less than that in MSNRhNPs with smaller particle size. The higher selectivity to C_2 oxygenates of

MSNRhNPs might be related to both Rh particle size and the special interaction between MSN matrix and RhNPs, which is still under investigated in our lab.

After being modified with promoter Mn^{n+}, as shown in Table 1, MSNRhNPs-Mn had the highest selectivity (32.4 %) to ethanol and lowest selectivity (3.7 %) to methanol. And both MSNRhNPs-Mn and Rh-Mn-MSN have higher catalytic activities after being modified with Mn^{n+} than that of their unmodified counterparts MSNRhNPs and Rh-MSN respectively (Entry 3 and 4 in Table 1). That indicates that manganese oxides not only can improve the selectivity of Rh catalysts to C_2 oxygenates but also can accelerate the CO hydrogenation. In another words, Mn^{n+} not only help to tilt the adsorbed CO from Rh to Mn which is helpful to synthesize ethanol and acetaldehyde according to Bao et. al.,[58] but also participate the hydrogenation of CO to HCO which was thought to be the rate limiting step in CO hydrogenation to ethanol according to the density functional theory.[60] Although the mechanism of Mn effects on CO hydrogenation is still under investigation, it is clear that the close interaction between Rh and Mn is necessary for a better catalytic performance of Rh catalyst in CO hydrogenation, which was further proved by our catalytic tests over MSNRhNPsMn.

As listed in Table 1 (Entry 4 and 5), the catalytic activity of MSNRhNPsMn was almost the same as that of MSNRhNPs-Mn, which is because the same RhNPs were used as the catalytic sites in both cases. Although the selectivities to gas product methane were close to each other for MSNRhNPsMn and MSNRhNPs-Mn, interestingly, the selectivity of MSNRhNPsMn to ethanol is much higher than that of MSNRhNPs-Mn as shown in Figure 5. Methanol, which usually is one of the main liquid by-products in CO hydrogenation, was kept at very low level through our tests when MSNRhNPsMn was used as catalyst. In the

mean time, CO_2 production is under GC's detection limitation even at 593 K for MSNRhNPsMn as well. These results indicate that the closer or stronger interaction between promoter Mn and catalytic site Rh is necessary to synthesize the ideal product C_2 oxygenates such as ethanol and suppress the formation of by-product methanol. As shown in Figure 5, the selectivity of ethanol in tested temperature range from 523 K to 573 K reached its highest point and the selectivity of methane touched its lowest point although the CO conversion is only around 9.8 % which is lower than 24.2 % at 543 K.

Conclusions

In summary, we have designed a new Rh-based catalyst in which well-defined rhodium nanoparticles were distributed homogeneously through the whole mesoporous silica particle and could be easily modified by promoters during *in situ* of the formation of mesoporous silica. The resulting catalyst possesses a high surface area and narrow pore size distribution as normal MSN does. The new manganese modified rhodium catalyst could suppress the formation of by-product methanol efficiently therefore has very high selectivity to the ideal C_2 oxygenates in CO hydrogenation. With the demonstrated better thermostability and better catalytic performance of MSN-encapsulated and Mn-modified rhodium nanoparticles, we defined a novel synthesis and modification method for metallic heterogeneous catalysts.

Acknowledgement

This research was supported at Ames Laboratory by the U.S. DOE, office of BES, under contract DE-AC02-07CH11358.

References

1. Farrell, A. E.; Plevin, R. J.; Turner, B. T.; Jones, A. D.; O'Hare, M.; Kammen, D. M. *Science (Washington, DC, U. S.)* **2006**, *311*, 506-508.

2. Fang, K.; Li, D.; Lin, M.; Xiang, M.; Wei, W.; Sun, Y. *Catal. Today* **2009**, *147*, 133-138.

3. Subramani, V.; Gangwal, S. K. *Energy Fuels* **2008**, *22*, 814-839.

4. Spivey James, J.; Egbebi, A. *Chem. Soc Rev* **2007**, *36*, 1514-1528.

5. Takeuchi, K.; Matsuzaki, T.; Arakawa, H.; Sugi, Y. *Appl. Catal.* **1985**, *18*, 325-334.

6. Bhasin, M. M.; Bartley, W. J.; Ellgen, P. C.; Wilson, T. P. *J. Catal.* **1978**, *54*, 120-128.

7. Chuang, S. S. C.; Stevens, R. W., Jr.; Khatri, R. *Top. Catal.* **2005**, *32*, 225-232.

8. Takeuchi, K.; Matsuzaki, T.; Arakawa, H.; Hanaoka, T.; Sugi, Y. *Appl. Catal.* **1989**, *48*, 149-157.

9. Sugi, Y.; Takeuchi, K.; Matsuzaki, T.; Arakawa, H. *Chem. Lett.* **1985**, 1315-1318.

10. Kintaichi, Y.; Kuwahara, Y.; Hamada, H.; Ito, T.; Wakabayashi, K. *Chem. Lett.* **1985**, 1305-1306.

11. Zaman, S. F.; Smith, K. J. *Catal. Commun.* **2009**, *10*, 468-471.

12. Subramanian, N. D.; Balaji, G.; Kumar, C. S. S. R.; Spivey, J. J. *Catal. Today* **2009**, *147*, 100-106.

13. Spivey, J. J.; Egbebi, A. A.; Subramanian, N.; Kumar, N.; Gupta, M. *Prepr. Symp. - Am. Chem. Soc., Div. Fuel Chem.* **2009**, *54*, 127-128.

14. Shi, X.-R.; Jiao, H.; Hermann, K.; Wang, J. *J. Mol. Catal. A: Chem.* **2009**, *312*, 7-17.

15. Gupta, M.; Spivey, J. J. *Catal. Today* **2009**, *147*, 126-132.

16. Jiang, D.; Ding, Y.; Pan, Z.; Li, X.; Jiao, G.; Li, J.; Chen, W.; Luo, H. *Appl. Catal., A* **2007**, *331*, 70-77.

17. Budge, J. R.; Gates, B. C. **1982**, *1*, 204-207.

18. Terreros, P.; Fandos, R.; Granados, M. L.; Otero, A.; Rojas, S.; Vivar-Cerrato, M. A. *Stud. Surf. Sci. Catal.* **2000**, *130D*, 3891-3896.

19. Hanaoka, T.; Kim, W.-Y.; Kishida, M.; Nagata, H.; Wakabayashi, K. *Chem. Lett.* **1997**, 645-646.

20. Ito, S.-i.; Chibana, C.; Nagashima, K.; Kameoka, S.; Tomishige, K.; Kunimori, K. *Appl. Catal., A* **2002**, *236*, 113-120.

21. Burch, R.; Hayes, M. J. *J. Catal.* **1997**, *165*, 249-261.

22. Jiang, D.; Ding, Y.; Pan, Z.; Chen, W.; Luo, H. *Catal. Lett.* **2008**, *121*, 241-246.

23. Pan, X.; Fan, Z.; Chen, W.; Ding, Y.; Luo, H.; Bao, X. *Nat. Mater.* **2007**, *6*, 507-511.

24. Bastein, A. G. T. M.; Van der Boogert, W. J.; Van der Lee, G.; Luo, H.; Schuller, B.; Ponec, V. *Appl. Catal.* **1987**, *29*, 243-260.

25. Van der Lee, G.; Ponec, V. *J. Catal.* **1986**, *99*, 511-512.

26. Panpranot, J.; Goodwin, J. G., Jr.; Sayari, A. *J. Catal.* **2002**, *211*, 530-539.

27. Martinez, A.; Prieto, G. *Top. Catal.* **2009**, *52*, 75-90.

28. Ma, H.; Yuan, Z.; Wang, Y.; Bao, X. *Surf. Interface Anal.* **2001**, *32*, 224-227.

29. Mo, X.; Gao, J.; Goodwin, J. G. *Catal. Today* **2009**, *147*, 139-149.

30. Haider, M. A.; Gogate, M. R.; Davis, R. J. *J. Catal.* **2009**, *261*, 9-16.

31. Subramanian, N.; Spivey, J. J.; Gao, J.; Mo, X.; Goodwin, J. G.; Torres, W., Jr. *Proc. - Annu. Int. Pittsburgh Coal Conf.* **2008**, *25th*, 182/1-182/7.

32. Chen, W.; Ding, Y.; Jiang, D.; Pan, Z.; Luo, H. *J. Nat. Gas Chem.* **2005**, *14*, 199-206.

33. Yin, H. M.; Ding, Y. J.; Luo, H. Y.; Chen, W. M.; Lin, L. W. *Stud. Surf. Sci. Catal.* **2004**, *147*, 421-426.

34. Ojeda, M.; Granados, M. L.; Rojas, S.; Terreros, P.; Garcia-Garcia, F. J.; Fierro, J. L. G. *Appl. Catal., A* **2004**, *261*, 47-55.

35. Yin, H.; Ding, Y.; Luo, H.; Zhu, H.; He, D.; Xiong, J.; Lin, L. *Appl. Catal., A* **2003**, *243*, 155-164.

36. Yin, H.; Ding, Y.; Luo, H.; Yan, L.; Wang, T.; Lin, L. *Energy Fuels* **2003**, *17*, 1401-1406.

37. Luo, H. Y.; Zhang, W.; Zhou, H. W.; Huang, S. Y.; Lin, P. Z.; Ding, Y. J.; Lin, L. W. *Appl. Catal., A* **2001**, *214*, 161-166.

38. Luo, H.; Zhou, H.; Lin, L.; Liang, D.; Li, C.; Fu, D.; Xin, Q. *J. Catal.* **1994**, *145*, 232-234.

39. Gallaher, G. R.; Goodwin, J. G., Jr.; Huang, C. S.; Houalla, M. *J. Catal.* **1993**, *140*, 453-463.

40. Gallaher, G. R.; Goodwin, J. G., Jr.; Guczi, L. *Appl. Catal.* **1991**, *73*, 1-15.

41. Gallaher, G.; Goodwin, J. G., Jr.; Huang, C. S.; Houalla, M. *J. Catal.* **1991**, *127*, 719-731.

42. Chuang, S. S. C.; Pien, S. I.; Narayanan, R. *Appl. Catal.* **1990**, *57*, 241-251.

43. Van der Lee, G.; Schuller, B.; Post, H.; Favre, T. L. F.; Ponec, V. *J. Catal.* **1986**, *98*, 522-529.

44. Thomas, J. M.; Thomas, J. W.; Editors *Principles and Practice of Heterogeneous Catalysis*, 1996.

45. Satterfield, C. N. *Heterogeneous Catalysis in Industrial Practice. 2nd Ed*, 1991.

46. Le Page, J. F. *Applied Heterogeneous Catalysis: Design, Manufacture, Use of Solid Catalysts*, 1987.

47. Zhou, S.; Zhao, H.; Ma, D.; Miao, S.; Cheng, M.; Bao, X. *Z. Phys. Chem. (Muenchen, Ger.)* **2005**, *219*, 949-961.

48. Huang, Y.; Li, Y.; Hu, J.; Cheng, P.; Chen, H.; Li, R.; Li, X.; Yip, C. W.; Chan, A. S. C. *J. Mol. Catal. A: Chem.* **2002**, *189*, 219-224.

49. Huang, Y.; Chen, J.; Chen, H.; Li, R.; Li, Y.; Min, L. e.; Li, X. *J. Mol. Catal. A: Chem.* **2001**, *170*, 143-146.

50. Beck, J. S.; Vartuli, J. C.; Roth, W. J.; Leonowicz, M. E.; Kresge, C. T.; Schmitt, K. D.; Chu, C. T. W.; Olson, D. H.; Sheppard, E. W.; et al. *J. Am. Chem. Soc.* **1992**, *114*, 10834-10843.

51. Kresge, C. T.; Leonowicz, M. E.; Roth, W. J.; Vartuli, J. C.; Beck, J. S. *Nature (London)* **1992**, *359*, 710-712.

52. Song, H.; Rioux, R. M.; Hoefelmeyer, J. D.; Komor, R.; Niesz, K.; Grass, M.; Yang, P.; Somorjai, G. A. *J. Am. Chem. Soc.* **2006**, *128*, 3027-3037.

53. Ferrando, R.; Jellinek, J.; Johnston, R. L. *Chem. Rev. (Washington, DC, U. S.)* **2008**, *108*, 845-910.

54. Crooks, R. M.; Lemon, B. I., III; Sun, L.; Yeung, L. K.; Zhao, M. *Top. Curr. Chem.* **2001**, *212*, 81-135.

55. Crooks, R. M.; Zhao, M.; Sun, L.; Chechik, V.; Yeung, L. K. *Acc. Chem. Res.* **2001**, *34*, 181-190.

56. Grass, M. E.; Joo, S. H.; Zhang, Y.; Somorjai, G. A. *J. Phys. Chem. C* **2009**, *113*, 8616-8623.

57. Huang, W.; Kuhn, J. N.; Tsung, C.-K.; Zhang, Y.; Habas, S. E.; Yang, P.; Somorjai, G. A. *Nano Lett.* **2008**, *8*, 2027-2034.

58. Wang, Y.; Luo, H.; Liang, D.; Bao, X. *J. Catal.* **2000**, *196*, 46-55.

59. Hu, J.; Wang, Y.; Cao, C.; Elliott, D. C.; Stevens, D. J.; White, J. F. *Catal. Today* **2006**, *120*, 90-95.

60. Choi, Y. M.; Liu, P. *J. Am. Chem. Soc.* **2009**, *131*, 13054-13061.

Tables and Figures

Table 1. Catalytic data of Rh-based catalysts in CO hydrogenation*

		CO conversion (%)	Selectivity (%)				
			CH_4	CO_2	CH_3OH	C_2	C_{2+}
1	Rh-MSN	2.7	40.8	0	24.4	33.0	34.8
2	MSNRhNPs	4.8	27.2	0	17.8	53.0	55.0
3	Rh-Mn-MSN	13.7	63.0	1.6	3.8	24.3	31.6
4	MSNRhNPs-Mn	20.2	47.0	2.5	3.7	42.2	46.8
5	MSNRhNPsMn	24.2	51.2	0	0	40.3	48.8

* All data were collected at the same conditions (0.3 g of catalyst with 3.0 g SiC, 300 ^{o}C, 450 psi, 11 mL/min of CO, 22 mL/min of H_2).

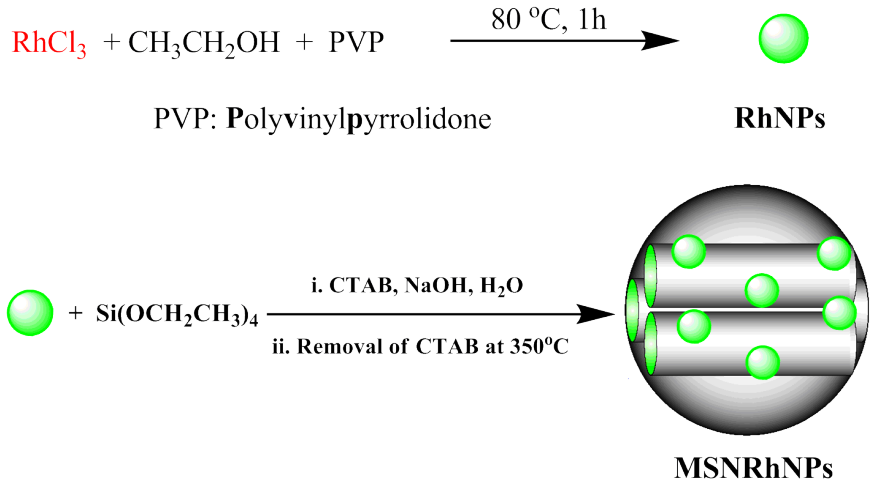

Figure 1-1. Synthesis of PVP-stabilized Rhodium Nanoparticles and the Subsequent Encapsulation of the RhodiumNanoparticle in the Framework of Mesoporous Silica Nanoparticles.

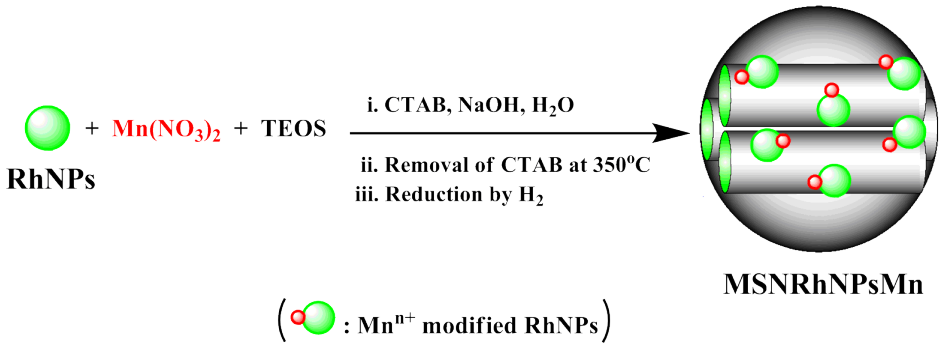

Figure 1-2. Synthesis of MSNRhNPsMn by co-condensation of $Mn(NO)_2$, RhNPs with TEOS.

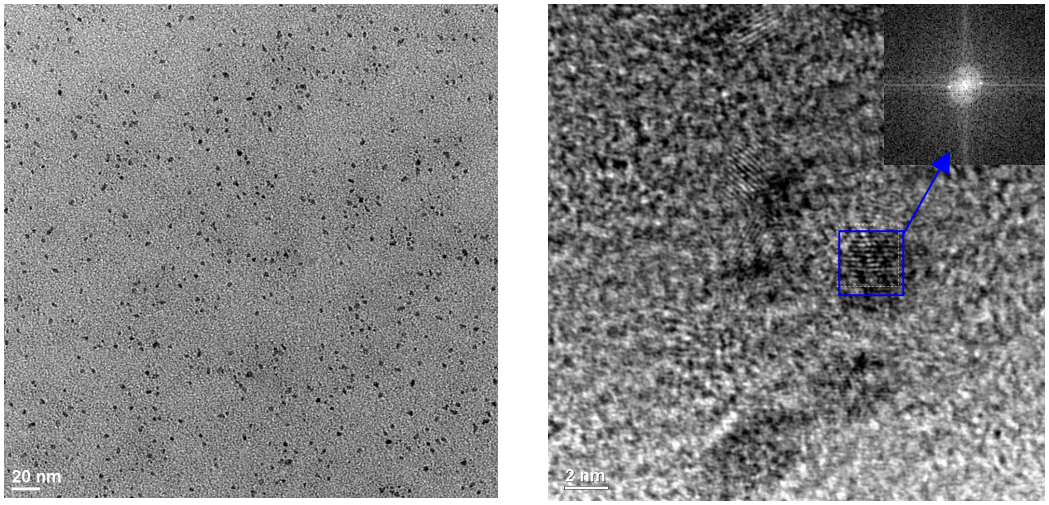

(a) **(b)**

Figure 2-1. TEM image (a) and HRTEM image (b) of RhNPs.

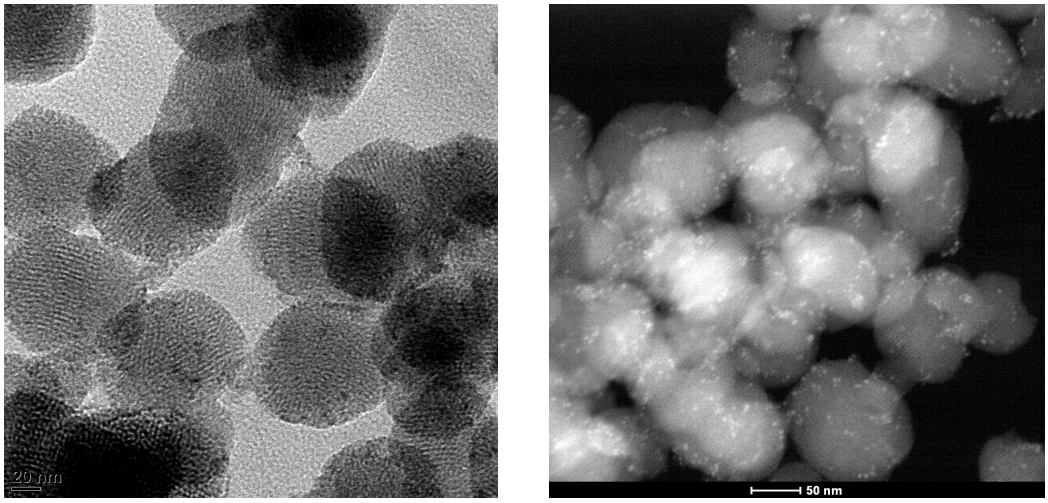

(a) **(b)**

Figure 2-2. TEM image (a) and STEM image (b) of MSNRhNPs.

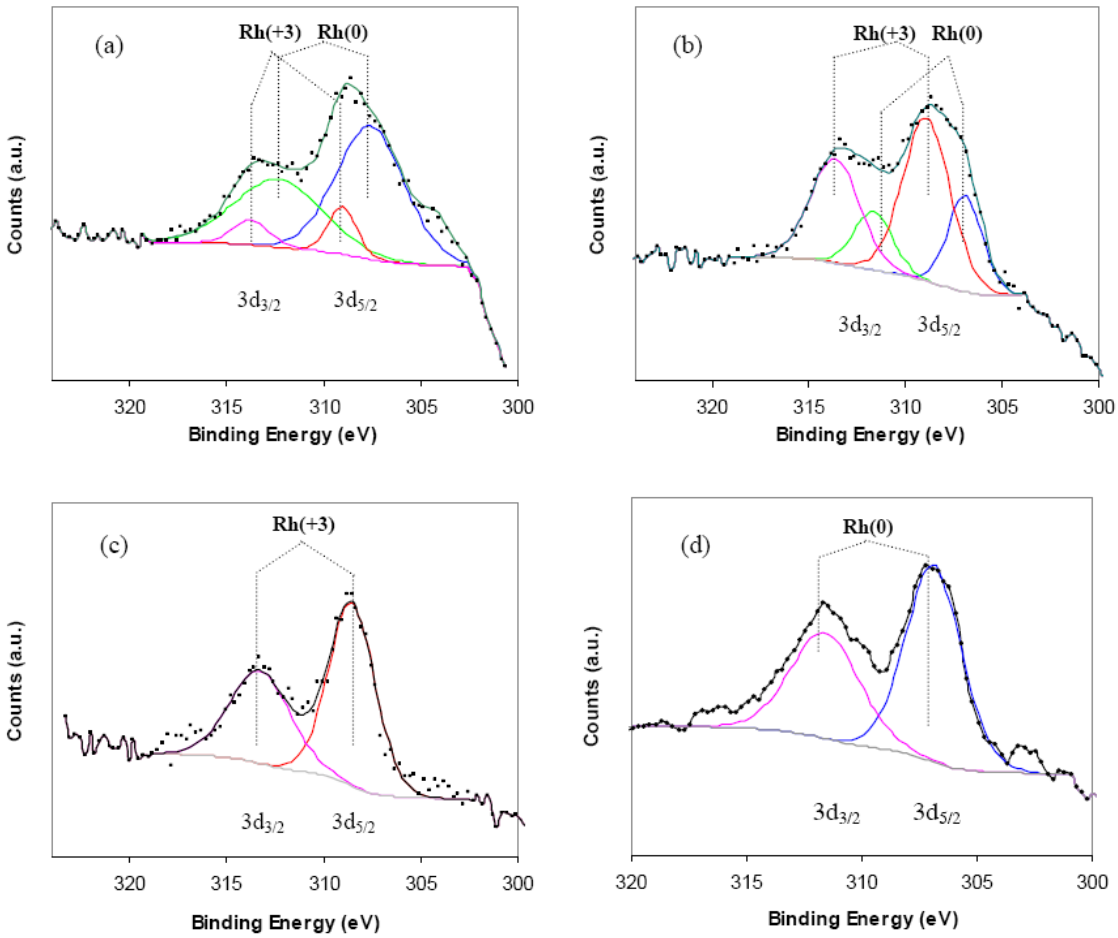

Figure 3. XPS of RhNPs (a) and MSNRhNPs (b): before calcination, (c): after calcination, (d): after reaction.

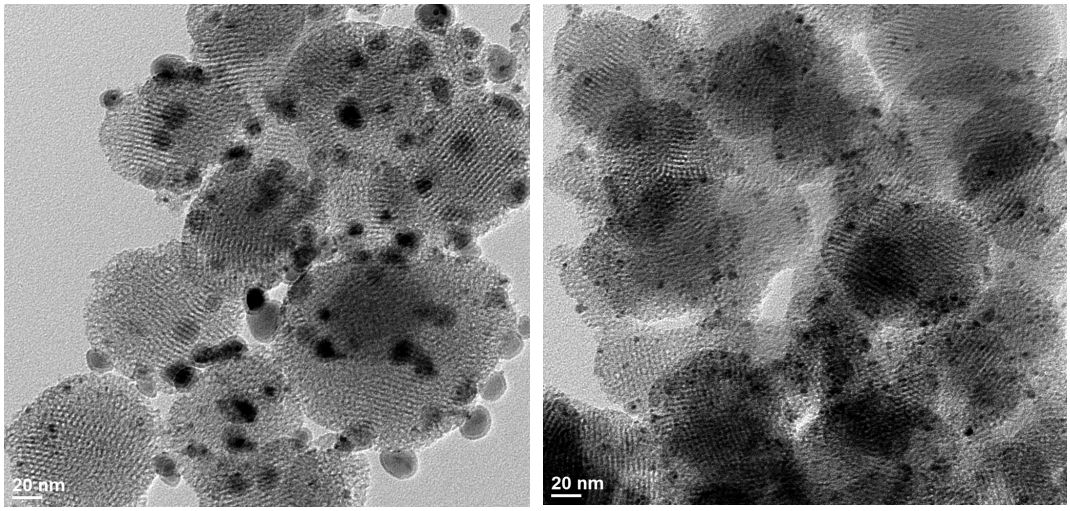

(a) **(b)**

Figure 4. TEM images of Rh-MSN (a) and MSNRhNPs (b) both after reaction at 300 ^{o}C for 24h.

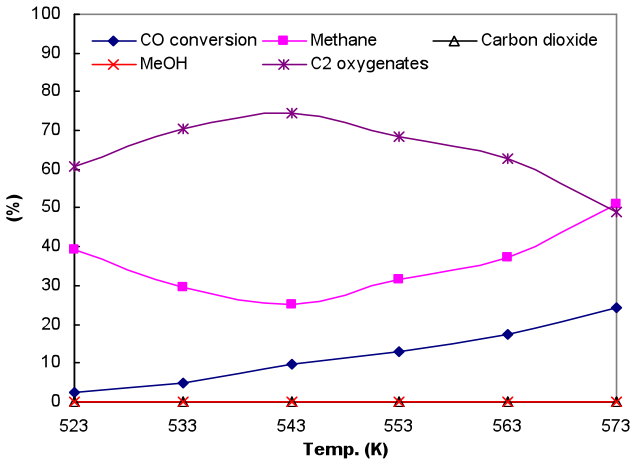

Figure 5. Effect of temperature on CO hydrogenation catalyzed by MSNRhNPsMn.

CHAPTER 3. ANIONIC SURFACTANT TEMPLATED MESOPOROUS CALCIUM SILICATE FOR TRANSESTERIFICATION REACTION OF TRIGLYCERIDE TO BIODIESEL

One section of a paper that has been accepted by *Topics in Catalysis,* reorganized

Enruo Guo, Chih-Hsiang Tsai, and Victor S.-Y. Lin*

Department of Chemistry, U.S. Department of Energy Ames Laboratory,

Iowa State University, Ames, Iowa 50011-3111, U.S.A.

**Corresponding author*

Abstract

Anionic surfactants are widely used for many industrial applications because of their environmental friendliness and low cost. We have developed a phosphoric acid monoester based anionic surfactant as the structure directing agent for the synthesis of a novel mesoporous calcium silicate material. The synthetic mechanism for the self-assembly was investigated, via $S^-M^+I^-$ route (S^-: surfactant, M^+: metal ion, I^-: silicate). N_2 sorption analysis shows it has a high surface area. Other structure characterization was performed, such as XRD, TEM, EDS. Furthermore, the material is an excellent heterogeneous solid catalyst for transesterification reaction of soybean oil to biodiesel. Quantitative conversion can be achieved within 2 hours. It can be recycled 8 times without any decrease in reactivity.

Keywords: Mixed oxides, calcium silicate materials, heterogeneous catalysts, biodiesel, transesterification

Introduction

Biodiesel, also known as Fatty Acid Methyl Esters (FAME), is one of the promising alternative biofuels that can be easily produced by a base-catalyzed transesterification reaction with triglycerides and methanol.[1] Current industrial processes for biodiesel production are typically conducted by blending various oil feedstocks with methanol in the presence of sodium methoxide, sodium hydroxide, or potassium hydroxide as homogeneous catalysts.[1] While these strong bases are effective in catalyzing the transesterifcation reaction of triglycerides and methanol giving rise to high yields of FAME and glycerol, the current method of removing these toxic and corrosive chemicals from the product mixtures often requires neutralization with acids, extensive water washing and drying after separation of glycerol.[1] This tedious post-treatment process unavoidably raises the operational cost for biodiesel production and brings complication to the quality of FAME and glycerol. Several undesired side products, such as soaps, and un-reacted strong bases and acids are often detected in the mixture of final products. Up to 4 liters of water is needed for post-treating one litter of biodiesel produced from these homogeneous base-catalyzed reactions, and vacuum drying of the product at elevated temperature is usually needed after the washing process for removing residual water to ensure the desired self-life of FAME.

We recently reported on the development of a series of mesoporous calcium silicate solid materials that could efficiently catalyze the transesterification reactions of various oils with methanol for producing high quality of biodiesel with excellent catalyst recyclability and reusability.[2] The sysnthesis of those catalysts was based on the interaction of the positively charged CTAB binding to the hydrolyzed anionic silicates in aqueous solution, which is a crucial step for the formation of structurally ordered mesoporous silica materials,

such as MCM-41 silica.[5,6] The major advantage of these solid catalysts is that no energy-intensive post-treatments are needed. Also, we demonstrated that the mesoporous calcium silicate family could work with soybean oil (SBO). While these catalysts could indeed facilitate the transesterification reaction under mild condition, i.e., refluxing methanol and atmospheric pressure, the reaction kinetics was not as fast as those of the homogeneous catalysts, such as sodium methoxide and sodium hydroxide.

To replace the homogeneous catalysts in the current production processes of biodiesel, the reaction kinetics of tranesterification catalyzed by these solid mixed oxides would need to be further accelerated, while maintaining the cost-effectiveness and ease of preparation. Herein, we report on the synthesis and characterization of anionic surfactant templated calcium silicate mixed oxide materials. The catalytic performances of these materials for biodiesel production are also investigated. As detailed in the following sections, we describe the fine-tuning of experimental variables for the synthesis of calcium silicate materials for significantly improving the reaction kinetics.

Experimental

1.1 Chemicals and Materials

Calcium hydroxide $Ca(OH)_2$, sodium hydroxide (NaOH), hydrogen chloride (HCl), methanol, and acetone were purchased and used as received from Fisher, Inc. Solid sodium silicate powder was obtained from PQ Corporation. Tetraethylorthosilicate (TEOS), tetraethylene glycol, phosphorus oxychloride and 11-bromoundec-1-ene were purchased from Sigma-Aldrich. Degummed soybean oil was obtained from West Central Co-op.

1.2 Deverlopment and Preparation of Phosphoric Acid Monoester-Directed Mesoporous Calcium Silicate (PMCS) catalysts

In addition to tuning the synthetic condition for the calcium silicate mixed oxide materials, an anionic surfactant, phosphoric acid monoester (PME) surfactant, 3,6,9,12-tetraoxatricos-22-enyl dihydrogen phosphate, was prepared according to the reported literature and used as the structure-directing agent for the synthesis of another series of mesoporous calcium silicate materials via the aforementioned co-condensation reaction. In this case, PME served as the surfactant (S^-) micelles templates, calcium (metal ion, M^+) ions and then hydrolyzed TEOS (inorganic precursor, I^-) coordinate accordingly, based upon electrostatic interactions, in the $S^-M^+I^-$ system [3, 4] The PME surfactant in 100 mL of water was heated to 80 °C. The basicity of the PME solution was then adjusted to pH 11.5, followed by the addition of TEOS (1 mL). Solid calcium hydroxide was then gradually added to the mixture. The reaction was carried out at 80 °C for 1 h under vigorous stirring, followed by aging at 90 °C for 24 h. The resulting solid product was collected by hot filtration and washed with copious amount of water and methanol. The PME surfactant was removed by calcination at 600 °C for 6 h.

1.3 Transesterification of soybean oil to biodiesel

In order to correctly evaluate the catalytic ability of these calcium silicate materials, we followed the experiment procedures that were reported previously.[2] The procedures for the transesterification of soybean oil are as follows. The mixture of 200 mg of a dried solid catalyst and 24 mL of methanol was stirred for 20 min to uniformly disperse the particles. Soybean oil (1.0 g) was then added into the suspension of catalyst in methanol. The reaction mixture was stirred at refluxing methanol temperature (64.7 °C) under atmospheric pressure.

After the complete conversion of oil to FAME was reached, the product mixture was filtered by a glass frit to separate the catalyst from the liquids.

Methanol was evaporated under vacuum. $CDCl_3$ was added to the remaining liquid for ^1H NMR analysis. The conversion percentage of transesterification reaction was analyzed by measuring the ratio of methyl protons (~3.6 ppm) to methylene hydrogens (α protons next to carbonyl group, 2.3 ppm).

1.4 Material Characterization and Analysis

Powder X-ray diffraction patterns of these PMCS materials were measured by Scintag Powder X-ray instrument. Micromeritics ASAP and Tristar apparatuses were used for nitrogen sorption isotherms, BET, and BJH measurements. Chemisorption of materials was measured using Micromeritics AutoChem II. TEM micrographs were obtained by using Tecnai G2 F20 Transmission Electron Microscope.

Results and Discussions

2.1 Synthesis and Catalytic Properties of PMCS

Anionic surfactants that can be self-assembled into micelles in water have been used as structure-directing templates for the synthesis of mesoporous silica materials.[3, 9-13] In our study, positively charged calcium ions were introduced to interact with the phosphate groups of the anionic PME surfactant molecules as described previously. Under basic conditions, hydrolyzed TEOS easily coordinates with the calcium/surfactant in a $S^-M^+I^-$ complex system and forms ordered structure.[3] After the removal of surfactants, the calcium sites would be exposed to the surface and therefore could react with methanol and feedstock effectively. Table 3 summarized the different conditions for the preparation of PME-templated calcium

silicate mixed oxide catalysts (PMCS 1-9). First, we synthesized materials (PMCS 1-3) by using lower amounts of calcium hydroxide under various pH conditions and they showed little or no catalytic reactivity for transesterification.

We then increased the amounts of $Ca(OH)_2$ gradually at pH 11.5, and the PMCS started to exhibit catalytic reactivity for transformation. As shown in Figure 1, when the amount of calcium hydroxide was doubled, the PMCS-4 catalyzed transesterification of SBO to biodiesel could be completed in 10 h. We further increased the amount of calcium, the reactivity was dramatically improved and only 2 h was needed to reach the 100% yield in the case of PMCS-5. Interestingly, introducing more calcium hydroxide during the synthesis of material did not lead to any faster kinetics for biodiesel production. Contrarily, it took more than 20 hours to complete the reaction when we further increased the amount of calcium (PMCS-6). As stated previously, pH is an important factor for the synthesis of these mixed oxides. In the case of PMCS materials, we found that catalysts (PMCS-5, 8, 9) exhibited almost identical reactivity (complete conversion of SBO to FAME within 2 h) when pH was set in the range between 10.3 and 12.2. In contrast, the reactivity dropped rapidly and took 10 h to complete the reaction when pH was lowered to 9 during material synthesis for PMCS-7. While calcium oxide alone has been examined as a catalyst for transesterification of triglycerides to biodiesel,[7, 8] however, the high solubility in methanol makes this material a less attractive candidate for recyclable heterogeneous catalysis[8]. All PMCS catalysts could be reused for 8 times with similar reactivity after regenerated by calcination at 600 ^{o}C for 6 h. PMCS collected by direct filtration and lypholization after reaction did not yield good recyclability (~50% yield at 2 h for the second cycle). This could be attributed to the surface poisoning effect by reactant and/or product molecules.

Similar to previous literature reports on using the $S^-M^+I^-$ synthesis route,[3] our PMCS catalysts are comprised of a lamellar type of porous structure. Figure 2 (b) shows the low angle powder X-Ray diffraction patterns of the PMCS materials. PMCS-3, which is with the lowest calcium loading, exhibited three strong peaks (d_{100}, d_{200}, and d_{300}) that are characteristic of a well-ordered lamellar structure. As the Ca/Si ratio went up, these patterns decreased and eventually gone as in the case of PMCS-6. The X-Ray diffraction patterns at high angles of the PMCS-4, PMCS-5 and PMCS-6 catalysts possess peaks around 29~30° at 2θ as shown in Figure 2 (a). These peaks could be attributed to active calcium silicate catalyst layers, which were also observed in the previously reported mesoporous calcium silicate family.[2, 14] In particular, sharp peaks at 29° were observed in PMCS-4 and 5, whereas a slightly shifted and broad peak was noticed in the case of PMCS-6. These results suggested that this peak at 29° is responsible for the high catalytic reactivity. The difference in X-ray diffraction patterns correlate well with their catalytic reactivities, i.e., no peak at 29° could be observed in PMCS-3, which is a material that showed no reactivity for transesterification. Also, PMCS-3 and PMCS-4 both exhibited a peak at 26°, which could be attributed to the formation of hydroxyapatite, which is not resposible for the catalytic reactivity. At the same time, PMCS catalysts showed no presence of characteristic peaks from calcium oxide, indicating that there are not discrete crystalline calcium oxide sites present, but a structure in which calcium is incorporated into the matrix of the material. As depicted in Figure 3, the nitrogen surface adsorption and desorption analysis of PMCS-5 revealed a type III mesostructure with a type H_3 hysteresis[15] further confirming a plate-like porous structure. The total surface area of the PMCS-5 catalyst is 150 m^2/g.

2.3 Chemisorption Properties of PMCS-5 Catalysts

The chemisorption measurement of the best catalyst (PMCS-5) is based on temperature-programmed-desorption (TPD) of surface-adsorbed pyridine on these catalysts. The results are summarized in Table 2. Pyridine desorption PMCS-5 occurred at 175.2 °C. The pyridine amounts obtained from the corresponding TPD curve is 0.38 mmol/g for PMCS-5, while the reference material, 250 nm bare silica bead, showed no absorption of pyridine. These results suggested that calcium silicate solid materials are more Lewis acidic than pure silica and are able to catalyze the esterification of free fatty acid to biodiesel as well. [2]

Conclusion

We have demonstrated the synthesis and characterization of a new type of calcium silicate mixed oxide catalysts for the efficient transesterification of soybean oil to biodiesel with high recyclability. PMCS-5, which is mesoporous calcium silicate catalyst with a lamellar porous structure, could be easily prepared by using a phosphoric acid monoester surfactant as template. We demonstrated that this PMCS-5 material efficiently catalyzed the transesterification of soybean oil to biodiesel within 2 h. This catalyst could be recycled and reused for 8 times after regeneration by calcination. Unlike the conventional sodium methoxide and hydroxide biodiesel catalysts that require neutralization and water washing, the heterogeneous nature of the recyclable calcium silicate mixed oxide catalysts that have been developed in this study can eliminate these tedious post-treatment processes. We believe that this research offers promising potential for significantly improving the current chemical process for biodiesel production.

References

1. Ma, F.; Hanna, M. A., *Bioresour. Technol.* **1999,** *70* (1), 1-15.

2. Lin, V. S.-Y.; Nieweg, J. A.; Verkade, J. G.; Reddy, C. R. V.; Kern, C. Mesoporous silicate-alkaline earth oxide composite catalysts for manufacture of biodiesel from fats and glycerides. 2008021232,2008.

3. Huo, Q.; Margolese, D. I.; Ciesla, U.; Feng, P.; Gier, T. E.; Sieger, P.; Leon, R.; Petroff, P. M.; Schueth, F.; Stucky, G. D., *Nature (London, U. K.)* **1994,** *368* (6469), 317-21.

4. Che, S.; Garcia-Bennett, A. E.; Yokoi, T.; Sakamoto, K.; Kunieda, H.; Terasaki, O.; Tatsumi, T., *Nat. Mater.* **2003,** *2* (12), 801-805.

5. Zhao, D.; Feng, J.; Huo, Q.; Melosh, N.; Frederickson, G. H.; Chmelka, B. F.; Stucky, G. D., *Science (Washington, D. C.)* **1998,** *279* (5350), 548-552.

6. Kresge, C. T.; Leonowicz, M. E.; Roth, W. J.; Vartuli, J. C.; Beck, J. S., *Nature (London, U. K.)* **1992,** *359* (6397), 710-12.

7. Reddy, C. R. V.; Oshel, R.; Verkade, J. G., *Energy Fuels* **2006,** *20* (3), 1310-1314.

8. Kouzu, M.; Yamanaka, S.-y.; Hidaka, J.-s.; Tsunomori, M., *Appl. Catal., A* **2009,** *355* (1-2), 94-99.

9. Garcia-Bennett, A. E.; Kupferschmidt, N.; Sakamoto, Y.; Che, S.; Terasaki, O., *Angew. Chem., Int. Ed.* **2005,** *44* (33), 5317-5322.

10. Gao, C.; Sakamoto, Y.; Sakamoto, K.; Terasaki, O.; Che, S., *Angew. Chem., Int. Ed.* **2006,** *45* (26), 4295-4298.

11. Garcia-Bennett, A. E.; Miyasaka, K.; Terasaki, O.; Che, S., *Chem. Mater.* **2004,** *16* (19), 3597-3605.

12. Gao, C.; Qiu, H.; Zeng, W.; Sakamoto, Y.; Terasaki, O.; Sakamoto, K.; Chen, Q.; Che, S., *Chem. Mater.* **2006,** *18* (16), 3904-3914.

13. Gao, C.; Sakamoto, Y.; Terasaki, O.; Che, S., *Chem.--Eur. J.* **2008,** *14* (36), 11423-11428.

14. Chen, J. J.; Thomas, J. J.; Taylor, H. F. W.; Jennings, H. M., *Cem. Concr. Res.* **2004,** *34* (9), 1499-1519.

15. Kruk, M.; Jaroniec, M., *Chem. Mater.* **2001,** *13* (10), 3169-3183.

Tables and Figures

Table 1. PMCS Catalysts synthesized by using the phosphate monoester surfactant template.

Entry No.	PME (mg)	$Ca(OH)_2$ (mg)	TEOS (mL)	H_2O (mL)	pH value
PMCS-1	185	37	1	100	3.4
PMCS-2	185	37	1	100	9.0
PMCS-3	185	37	1	100	11.5
PMCS-4	185	74	1	100	11.5
PMCS-5	185	148	1	100	11.5
PMCS-6	185	296	1	100	11.5
PMCS-7	185	148	1	100	9.0
PMCS-8	185	148	1	100	10.3
PMCS-9	185	148	1	100	12.2

Table 2. Chemisorption analysis of calcium silicate mixed oxide catalysts

Material	Pyridine absorbed (mmol/g)	Peak temp (°C)	Surface area (m^2/g)
Silica nanoparticles*	No peak	NA	10
PMCS-5	0.38501	175.2	150

* Colloidal silica with an average particle diameter of 250 nm synthesized by Stober method

** Pyridine adsorption at 120 °C. TPD program: 10 °C/min heating ramp from 120 to 600 °C, total duration for TPD is 2 h.

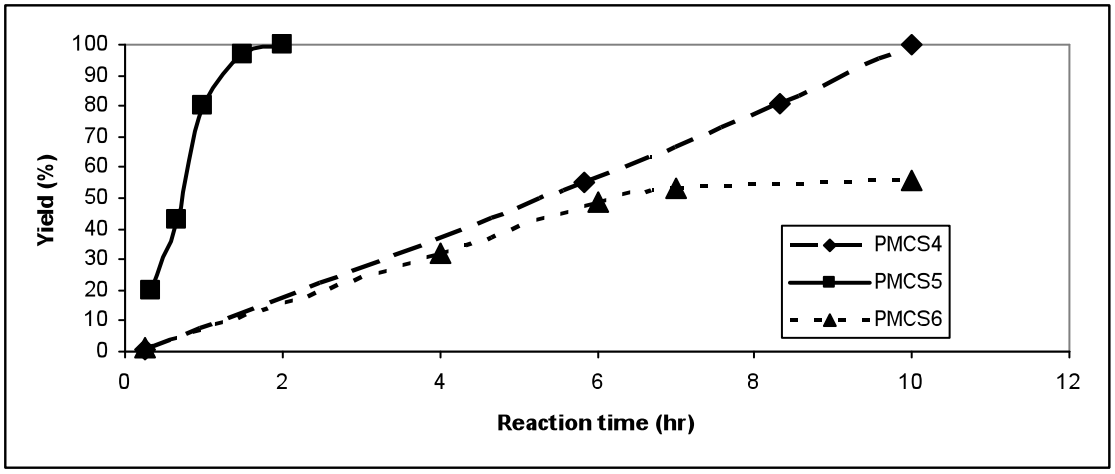

Figure 1. Reaction kinetics of the transesterification of soybean oil to biodiesel by PMCS catalysts with different calcium oxide amounts.

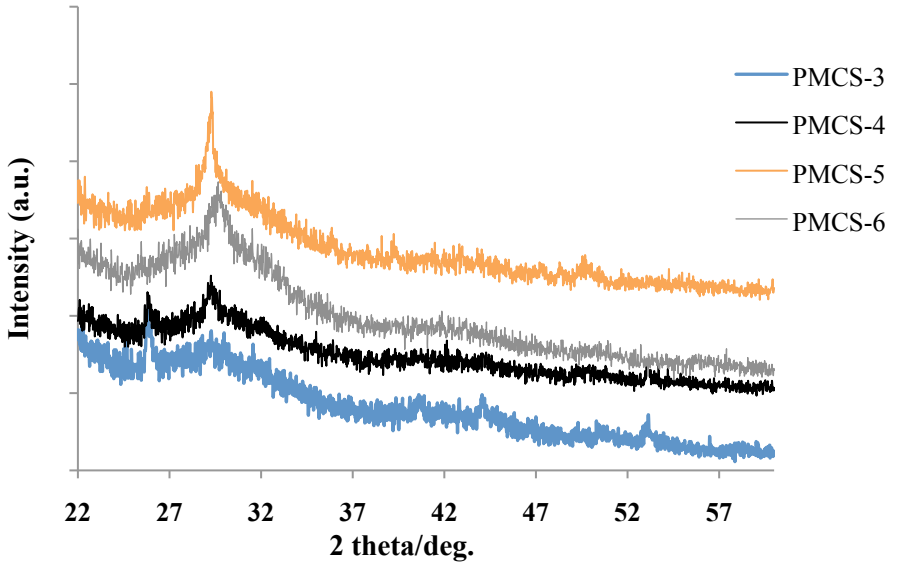

(a)

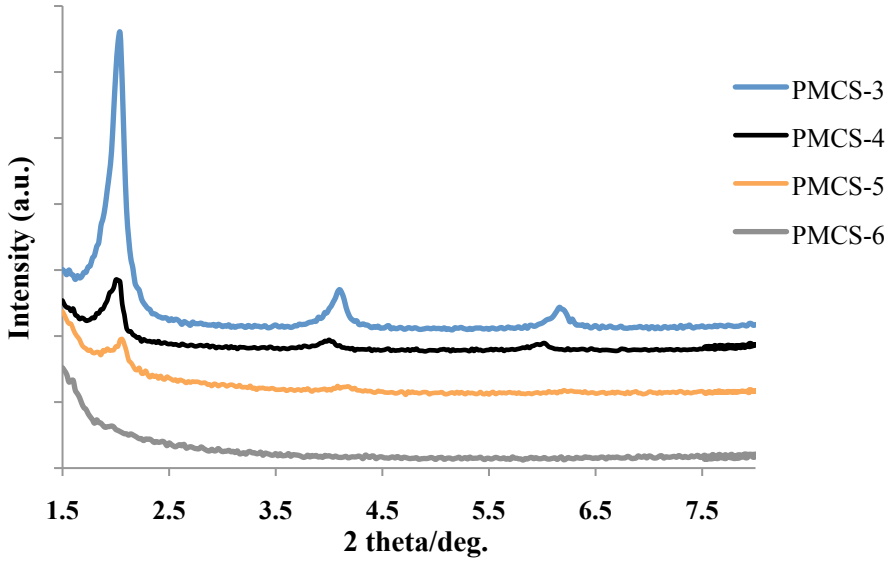

(b)

Figure 2. Powder X-ray diffraction patterns of PMCS catalysts at (a) low and (b) high angle.

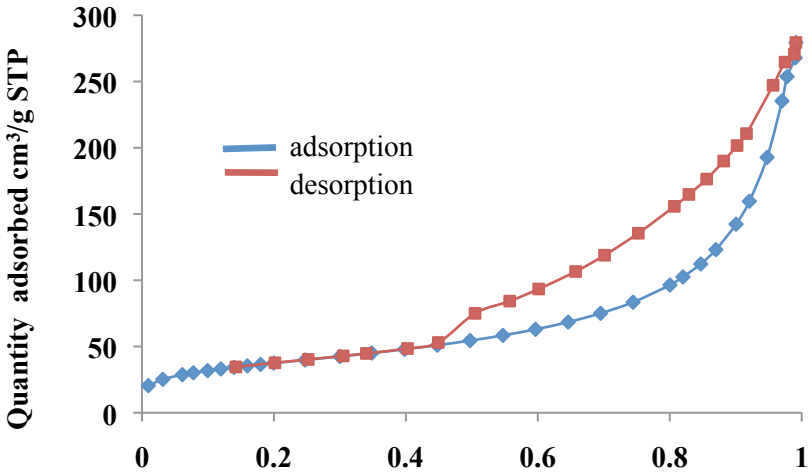

Figure 3. Nitrogen sorption isotherm of PMCS-5 catalyst.

CHAPTER 4. CERIA NANOPARTICLE LINKED MCM-41 TYPE MESOPOROUS SILICA MATERIAL: FREE RADICAL SCAVENGER AS WELL AS A CONTROLLED RELEASE VEHICLE

Enruo Guo, Yannan Zhao, Victor S. Y. Lin*

Department of Chemistry, Iowa State University, Ames, 50011-3111, U.S.

**Corresponding author*

Abstract

Triethoxysilyl propylsuccinic acid grafted ceria nanoparticles (TESSA-CNPs) were synthesized with particle size of 4-5 nm, and covalently linked with mesoporous silica nanomaterials (MSNs). A cleavable disulfide bond was employed as a stimuli responsive controlled release system. The ceria nanoparticles (CNPs) can effectively cap the mesopores of MSN, while the loaded drug can be triggered release from the mesopores after the addition of disulfide reducing agent. CNP-MSNs showed better reactive oxygen species (ROS) suppression properties than naked CNPs. This property was pH dependent. When skin fibroblast cells were treated with CNP-MSN, it showed improved viability versus cells treated with CNPs, when both were treated with doxorubicin. We found CNP-MSN has much better endocytosis efficiency than CNPs. Interestingly, HeLa cells were not protected from doxorubicin induced toxicity by either CNP-MSN or CNPs.

Introduction

Controlled-release of drugs based on mesoporous silica nanoparticles (MSN) with high surface area and tunable pore size is of keen interest. Our group has demonstrated

previously that MSN can serve as a drug delivery vehicle.[1-11] Drugs can be entrapped in the channel by multiple hard or soft caps. By introducing a drug release stimuli, it is possible to chemically cleave the bond between caps and MSN, or affect ligand exchange with the caps, drug release can be triggered from MSN. In 2003, we developed a CdS nanoparticles capped MSN as a stimuli-responsive controlled release system.[1] The CdS nanoparticles were chemically linked with MSN surface blocking the mesopores. The disulfide linkage between the caps and MSN can be cleaved with disulfide reducing agents, thus triggering the release of loaded drugs from MSN. However, the toxicity of CdS nanoparticles limits the further applications in vivo.

Cerium oxide nanoparticles have attracted various attentions in biological application recently.[12-17] Due to the oxygen vacancies on the surface of cerium oxide, it consists of two oxidation state: +3 and +4, and can flip-flop between the two during redox reactions.[18] It has been reported that ceria nanoparticles could inhibit the increase in the intracellular concentration of reactive oxygen species (ROS) of rat retina cell, and even prevent photoreceptor cell from light-induced degeneration in vivo.[13] Ceria nanoparticles can even mimic the catalytic activity of superoxide dismutase.[19] These activities come from the mixed oxidation state on ceria surface, and directly correlate with the ratio of Ce (+3) to Ce (+4). A higher concentration of Ce (+3) results in a better activity in superoxide scavenging process.[15] Early studies showed that a decrease in particle size, an increase in surface area to volume ratio, gives rise to a larger surface oxygen vacancy.[20] CNPs with particle size around 5 nm is able to regenerate and act as a catalyst.[13] However, other researchers found cytotoxicity and oxidative stress induced by cerium oxide with larger size (such as 20 nm) in cultured BEAS-2B cells[21] and human lung cancer cells.[22] Interestingly, researchers also

found a selective protection of normal cells by CNPs when treated with radiation or H_2O_2, but not to tumor cells.[12,16] The different protection may come from the intra- and extracellular pH differences presented in normal versus tumors tissue due to metabolic activity. [12, 16]

In order to overcome CdS nanoparticle induced cytotoxicity, we studied ceria nanoparticles (CNPs) as the mesopore caps as well as an antioxidant to scavenge reactive oxygen species. In our study, we first synthesized TESSA coated ceria (TESSA-CNP) with particle size around 4-5 nm by sol-gel method, and then chemically linked with linker-MSN by amidation reaction (CNP-MSN).[1] Dithiothreitol (DTT) was used to reduce the disulfide bond, breaking the connection of caps from MSN. At the first 2h, the release amount reached 60% of the total release, and arrived at the plateau after 35 hours. Also, release concentration exhibited DTT concentration dependent. CNP-MSN exhibited pH-dependent antioxidant property when exposed to H_2O_2. Interestingly, it was shown to suppress ROS even more efficiently than naked cerium oxide. We even investigated the property in cultured skin fibroblast cell. We found CNP-MSN could attenuate doxorubicin induced toxicity, which is well known as an intracellular ROS producer as well as an antitumor antibiotic.

Results and Discussion

First, we made the thiol-functionalized MSN by co-condensation of tetraethyl orthosilicate (TEOS) and mercaptopropyl trimethoxysilane (MPTMS) via our previously reported method.[23,24] After the removal of surfactant, we connected the 2-propyl-disulfanyl ethylamine to MSN through two-step thiol exchange reaction. At the same time, we made the TESSA grafted CNPs with particle size around 4-5 nm by sol-gel method modified from a

literature procedure.[25] The mesopores of MSN was used to encapsulate aqueous drug solution, and the openings of the mesopores were capped by allowing the TESSA-CNPs covalently bonded with the amine group through amidation reaction.

X-ray diffraction pattern of CNPs, Figure 15 (a) showed it crystallized in a fluorite structure. X-ray photoelectron analysis (Figure 15 (b)), verified that CNPs has both +3/+4 oxidation states, which are necessary for the redox chemistry.[19] Fourier transform infrared spectroscopy (Figure 16) further verified TESSA coated on ceria. The peak at 1710 cm^{-1} was indentified as the carboxylic carbonyl stretch from TESSA. Thermo gravimetric analysis (TGA, Figure 22) showed there was around 20% organic composite on CNPs.

X-ray diffraction (Figure 20) at small angle showed that the functionalized MSN still preserved hexagonal mesostructure found in unfunctionalized MSN. After capping with TESSA-CNPs, the diffraction pattern disappeared, indicating the mesopores were blocked by the caps. Nitrogen sorption isotherms showed that Brunauer–Emmett–Teller (BET) surface area decreased from 920 m^2/g to 320 m^2/g. Also, pore size distribution calculated by Barrett-Joyner-Halenda (BJH) method (Figure 21 (b)) showed the pores were blocked after capping. TGA (Figure 23) indicated the organic groups on MSN. Zeta potential (Table 1) measurement also verified the surface changes on MSN.

We investigated the stimuli responsive release by using fluorescein as a guest molecule. The total loading of fluorescein was found to be 11 μmol/g. Figure 1 (a) showed the triggered release profile. After a period of 24 h in PBS buffer solution (pH 7.4), the system exhibit less than 5% release, indicating a good capping efficiency. After the addition of DTT (18.5 mM) to the suspension, a release of entrapped fluorescein was triggered. After

35 hours, the release reached 100 % of the relative release. When compared to the loading amount, the total release is 34%.

We also varied the concentration of DTT, and found the release amount is DTT concentration dependent (see Figure 1 (b)). The amount of release is controlled by the amount of caps that being cleaved by DTT.

After demonstrating that CNP-MSN can serve as a controlled release system, we begin analyzing CNPs' antioxidant property, in order to find out if it can reduce ROS concentration. The 2',7'-dichlorfluorescein diacetate (H_2DCF-DA) is a well-established compound to detect and quantify intracellular produced reactive oxygen species. In the presence of ROS, the non-fluorescent H_2DCF-DA is oxidized to highly fluorescent DCF-DA (Figure 2). Herein, we used it as a probe to monitor the ROS generated by H_2O_2.

Figure 3 (a) shows the fluorescence intensity of DCF-DA changes with time. When H_2O_2 was added, an increase in fluorescence was observed, as shown in the blue line. When CNPs were in the suspension with H_2O_2, the fluorescence intensity was lower than that of experiments without CNPs, shown in green line. Most interestingly, CNP-MSN showed even lower fluorescence intensity than tests with CNPs alone. Since the compound H_2DCF-DA only turns fluorescence after being oxidized, the lower fluorescence intensity, the lower the ROS concentration. In other words, CNPs especially when linked with MSN, can effectively suppress the ROS generation induced by H_2O_2.

Based on our observations, the TESSA-CNPs were difficult to disperse in the buffer solution. Once connected with MSN, the CNP-MSN composite was easier to suspend. The high surface area and porous structure of MSN could help CNPs a better dispersion. As previously reported,[20] the particle size of ceria still played a role in its antioxidant properties,

the smaller of the size, the more oxygen vacancies it has, and the better ROS suppression ability it has. We believe that a better suspenstion would help CNPs to remain in a smaller size, a larger contact possibility with the reactant, and a better ROS consumption ability.

Basically, the mixture undergoes several reactions after the addition of H_2O_2 (see scheme below). The standard reduction potential of H_2O_2 / H_2O is 1.78 eV, while Ce^{4+} / Ce^{3+} is 1.44 eV, indicating that H_2O_2 can act as the oxidizer and oxidize Ce^{3+} to Ce^{4+}. At the same time, the standard reduction potential of HO_2 / H_2O_2 is 1.5 eV, meaning that Ce^{4+} has the ability to turn back to Ce^{3+} by getting one electron. HO_2 radical is thought to be of importance to convert Ce^{4+} back to Ce^{3+}.[26] However, in acidic condition, a higher concentration of protons may inhibit the reaction (2) to occur, thus H_2O_2 is likely to undergo half reaction (1).

$$H_2O_2 + 2H^+ + 2e^- \longrightarrow 2H_2O \quad 1.78\ eV \qquad (1)$$

$$H_2O_2 \longrightarrow HO_2 + e^- + H^+ \quad -1.5\ eV \qquad (2)$$

$$Ce^{4+} + e^- \longrightarrow Ce^{3+} \quad 1.44\ eV \qquad (3)$$

Perez et al. has reported the pH dependent antioxidant property of nanoceria.[16] They observed that in acidic condition, Ce^{4+} remained at a higher concentration after the addition of H_2O_2 in 10 days. In contrast, Ce^{4+} were able to turn to its original concentration in neutral or basic condition. As expected, the fluorescence intensity of CNP-MSN and CNPs exhibited quite similar trend compared with the H_2O_2-only one (Figure 3 (b)). These results verified that higher proton concentration has a negative effect on CNPs' capabilities as a ROS

scavenger. Furthermore, we found H_2O_2 induced H_2DCF-DA oxidation was faster in acidic condition, which verified the half reaction (1) was favored when pH was low.

In order to further compare the ROS consumption property of CNP-MSN with naked CNPs, we performed cell studies. First, we studied the cytotoxicity of both naked CNPs and CNP-MSN. Based on our previous study, MSN is nontoxic when concentration is below 100 μg/ml. Cell viability and proliferation was tested by treating with a series of concentrations of CNPs and CNP-MSN. As is shown in Figure 4, the experimental data suggests that CNP-MSN was biocompatible. When skin fibroblast and human cervix carcinoma cell (HeLa) was treated with CNP-MSN in concentrations from 10 to 30 μg/ml, a high viability as well as good proliferation was observed. Also, CNPs were not toxic in the concentration range from 1 μg/ml to 3 μg/ml.

Then we were trying to check the antioxidant property of CNP-MSN in cultured cells. Doxorubicin is a well known anticancer drug which has a large application in chemotherapy. The mechanism of DOX in cancer therapy is basically due to a high affinity in chelating and binding with DNA, interfering the cell division, and thus decreasing the cell proliferation in a large degree.[27] However, it's has been reported that DOX has some side effect to the normal tissue, such as cardiotoxicity, due to the production of reactive oxygen species (ROS) during its intracellular metabolism, which could be attenuated by antioxidant.[28]

Since DOX has a high affinity toward silica-based materials because of the electrostatic interaction, it's really hard to get DOX release profile in physiological condition based on our CNP-MSN system. In order to demonstrate if the CNP-MSN system can prevent or decrease the toxicity to normal cells induced by DOX, we did the cell experiment

by simply suspending CNP-MSN in the DOX solution. The cells were treated with the mixture and incubated for 24 hours.

Comparison of CNP-MSN and CNP was made based on the loading of CNP on MSN, which was quantified by ICP-MS. We did several experiments. First, we adjusted the concentration of the material, but kept the DOX solution at a certain level. Then, we varied the DOX concentration from 2 μM to 10 μM. When DOX concentration is at 2 μM (Figure 5) and 5 μM (Figure 6), respectively, we found the major effect of DOX was a sharp decrease in cell amount comparing with the untreated cells. While, the CNP-MSN treated cells exhibited better proliferation. After comparing with blank MSN, we suspect the behavior came from buffering effect of MSN. Due to the presence of MSN, there would have some changes in the intracellular DOX concentration, which later interfered the cell growth and cell amount. However, we didn't see an obvious difference in the cell viability between the free DOX solution and the CNP-MSN treated cells. The viability of cells treated with free DOX showed 80 % survival, while the CNP-MSN treated cells had 5-10 % higher percentage. An explanation is, at these relative low concentrations of DOX, ROS generated is not so distinct, that the cytotoxicity induced by ROS is not clear to see, and so is the protection effect from CNP-MSN. When we kept increasing DOX concentration to 10 μM (Figure 7), MSN's buffering effect was negligible, probably because the buffering has reached its limit. At this level, DOX was toxic enough and kill 70 % skin fibroblast cells. However, we found cell viability of the CNP-MSN treated cells was much higher than free DOX solution treated cells (Figure 7 (a)). And also this property is CNP-MSN concentration dependent. The higher of the concentration, a better survival of the treated cells. Then we performed skin fibroblast endocytosis experiment. EC_{50} of CNP-MSN was around 1.5 μg/ml,

indicating a good uptake efficiency (Figure 9, 11(a)). At concentration of 10 μg/ml, nearly 90 % of the cells have shown the fluorescence from FITC-labeled materials, while at 20 μg/ml, almost all the selected cells have the material. The results well explained the concentration dependent antioxidant property of CNP-MSN when mixed with DOX solution. The higher concentration of the CNP-MSN introduced, the higher of the intracellular concentration of this material, and a better scavenging property against DOX.

We further compared the antioxidant property of CNP-MSN with naked CNP, keeping the DOX concentration at 10 μM (Figure 7 (b)). To our surprise, the naked CNP was not as efficient to protect the cells as the CNP-MSN, even though it still showed higher live cell percentage comparing with free DOX solution. In order to investigate how this could happen, we checked the endocytosis efficiency of naked CNP (Figure 9, 11(b)). As we expected, the EC_{50} of naked CNP showed at 10 μg/ml, indicating naked CNP was much less favored than CNP-MSN. Other researchers also reported that cells prefer to uptake larger particles than smaller particles. Limbach et al.[29] studied the endocytosis of CNPs with a series of sizes by human lung fibroblast cells, and found larger ceria particles (250-500 nm) had better uptake efficiency than smaller particles (20-50 nm). Small nanoparticles underwent fast agglomeration upon contact to cell culture medium. The low density of the impaction-derived agglomerates reduced the ceria uptake per absorbed agglomerate, the diffusion coefficient, which contributed to a lower ceria uptake. However, larger nanoparticles with longer mean agglomeration time, could penetrate the cells more efficiently.

Endocytosis experiment is a strong evidence to verify the different scavenging efficiency of CNP-MSN and naked CNP. When the cells were treated with naked CNP at

concentration from 1 to 3 μg/ml, cells that real uptake the CNP was around 10 % of the total, meaning that the rest cells may suffer from ROS and other toxicity induced by DOX. The results also indicate the CNP's free radical scavenging process is inside the cells, and can only play a role when the CNP were uptake by the cells.

According to our H_2DCF-DA assay results, in acidic condition, CNP was unable to consume H_2O_2 and converted back to reduced oxidation state due to a high concentration of protons. As literature reported, ceria can preferentially protect the normal cells but not cancer cells which have an acidic micro-environment due to Warburg effect.[16] We wanted to see if CNP-MSN still preserves this pH-dependent antioxidant property.

We treated HeLa cells with a mixture of CNP-MSN and DOX solution. Figure 8 showed there was no protection against the toxicity induced by DOX. Interestingly, we found the difference of endocytosis efficiency of CNP-MSN and CNP by HeLa cells is less obvious than skin fibroblast. Figure 10 and 12 showed the EC_{50} of CNP-MSN treated cells is around 4 μg/ml, whereas 8 μg/ml for CNPs. Still, CNP-MSN has better ability to be uptake by HeLa than naked CNPs. Based on our understanding, this different uptake efficiency of CNP-MSN does play a role in the preferential protection of skin fibroblast cell, whereas non-protection to HeLa. Also, the lower pH environment in cancer cells that negatively affect the regeneration of Ce (+3) can still contribute to the non-protection to HeLa. Since cell is a complex system, other factors such as differential intercellular activity, differences in chromatin structure or free-radical targets, result in the different protection efficiency in normal cell and cancer cell[12]. In order to visually investigate the endocytosis by the cells, fluorescence confocal microscopy measurement was employed. As Figure 13 and 14 shows,

the naked CNPs had the tendency to form aggregations, while CNP-MSN was better suspended.

In summary, we successfully synthesized triethoxysilyl propylsuccinic acid grafted ceria nanoparticles linked-MSN, which can be served as a stimuli responsive drug delivery system as well as an efficient free radical scavenger. It showed pH dependent ROS consumption property. In particular, CNP-MSN showed a better function than naked CNPs when skin fibroblast cells were exposed to DOX. While, there was no protection to HeLa cells.

Experimental

Reagents and Materials. Cerium (III) nitrate hexahydrate (99%), 3-(mercaptopropyl) trimethoxysilane (MPTMS), 3-aminopropyltriethoxysilane (APTES), n-cetyltrimethylammonium bromide (CTAB), tetraethylorthosilicate (TEOS), 2,2'-dithiobispyridine, 2-aminoethanethiol hydrochloride, N-hydroxysuccinimide (NHS), 1-ethyl-3-(3-dimethylaminopropyl) carbodiimide (EDC), dithiothreitol (DTT), 3-(triethoxysilyl) propylsuccinic anhydride (TESSA), fluorescein, 2,7-dichlorofluorescein diacetate, fluorescein isothiocyanate (FITC), doxorubicin hydrochloride (≥98.0 %), ammonia solution (28.0 %-30.0 %), were purchased from Sigma-Aldrich and used as received. Hydrogen peroxide solution (30 % w/w) was purchased from Fluka. Nanopure water was prepared from a Barnstead E-pure water purification system.

Synthesis of ceria nanoparticles (CNPs). The synthetic routes were modified from literature.[25] 0.5M Ce^{3+} solution was prepared by dissolving $Ce(NO_3)_3.6H_2O$ in water/ethylene glycol 1:2 (v/v) co-solvent. Ammonia (30%) was diluted to 2M. Then 12 ml

diluted ammonium solution was added to the Ce^{3+} precursor solution under continuous stirring at room temperature. Immediately, brown yellow precipitate appeared. After stirring for 10 min, the precipitate was collected by centrifuge. And later washed with nanopure water three times and ethanol. Then the material was dried in lyophilizer.

TESSA grafted on CNPs. 0.11 g CNPs were suspended in 30 mL toluene. The mixture was sonicated for 30 min, until there's no big aggregation. Then TESSA (triethoxysilyl propylsuccinic anhydride) 0.13 mL (0.46 mmol) was added to the suspension. The temperature elevated to 110 ^{o}C, and kept reflux for 20 h. After centrifuge, the material was washed with methanol twice, and freeze drying.

Synthesis of MCM-41 type mesoporous silica nanoparticles functionalized with 2-(propyldisulfanyl) ethylamine (Linker-MSN). The synthetic methods were modified from our previous paper.[1] First we synthesized the mercaptopropyl functionalized MSN by co-condensation of MPTMS and TEOS.[23, 24] 1 g CTAB (2.7×10^{-3} mol) was dissolved in 480mL nanopure water, 3.5 mL NaOH (2 M) solution was then added, adjusting the temperature to 80 ^{o}C. 5 mL TEOS (2.6×10^{-2} mol) with 0.98 ml mercaptopropyl trimethoxysilane (5.2×10^{-3} mol) was introduced to the surfactant solution, stirring for 2 h. The afforded white precipitate was the as synthesized thio-MSN. After hot filtration, the material was washed with nanopure water and dried with methanol. In order to wash the surfactant template, 1 g as-synthesized material was reflux with 6 ml HCl (12M) in 100 ml MeOH, 60 ^{o}C, for 6 h. The remaining solvent was removed by loading the material in high vacuum. Then 0.888 g thio-MSN was treated with 0.392 g 2,2'-dithiobispyridine (mole ratio 1:2) in MeOH at room temperature under vigorous stirring for 24 h. The chemically accessible thiol group on MSN was calculated by UV absorption of the product (0.469

mmol/g). The product then underwent second thiol exchange reaction. The resulting MSN 0.8713 g was then stirred with 93 mg 2-aminoethanethiol hydrochloride (mole ratio 1:2) in MeOH at room temperature for 24 h. The material then was filtered, washed with methanol and dried in air.

Loading of fluorescein and capping with TESSA-CNPs on the mesopores. 50 mg MSN-linker was added in 10 ml 10^{-4} M fluorescein solution, sonicating for 20 min to get rid of air in the pores, and then incubated for 24 h. TESSA-CNPs 9.48 mg was suspended in 2ml 10^{-4} M fluorescein solution, followed by adding 9.2 mg NHS (N-hydroxysuccinimide) and 15.34 mg EDC (1-ethyl-3-(3-dimethylaminopropyl) carbodiimide). Then the above solution was added to the linker fluorescein solution. After stirring for 24 hours, the fluorescein loaded, TESSA-CNPs capped MSN was centrifuged, washed exclusively with nanopure water and dried in lyophilizer.

DTT induced fluorescein release. 10 mg loaded MSN was suspended in 5 mL PBS buffer solution (pH 7.4), stirring at RT. Fluorescence was used to monitor the any leaching and release. After 24 hrs, DTT (18.5 mM) was added to cleave the chemical bond between MSN and CNPs. The release kinetic profile was monitored by fluorescence with excitation wavelength at 480 nm and emission wavelength at 514 nm.

Reactive oxygen species measurement. Materials with different weight (the amount of CNPs used was based on the loading in CNP-MSN. Herein, 10 mg CNP-MSN, while 1 mg CNPs) were suspended in 10 ml buffer (pH 7.4 or pH 4), respectively, following the addition of 50 μL H_2O_2 (30 %). After 20 min incubation, 1 ml of the suspension was taken out and added to 10 ml H_2DCF-DA solution (20 μM). Fluorescence was measured with excitation wavelength at 504 nm, and emission wavelength at 524 nm in 0.1 M Tris buffer.

Since 2',7'-dichlorfluorescein diacetate can be oxidized and turned to fluorescent after being exposed in air , we prepared a H_2DCF-DA solution without adding any oxidizer as a control.

Cell culture. Skin fibroblast, HeLa cell lines were obtained from American Tissue Culture Collection (ATCC). Trypsin (1×, 0.25%) in 0.1 % EDTA-Na without calcium and magnesium was purchased from Fisher Scientific. All the cells were maintained in T75 flasks using the base medium DMEM (Dulbucco's modified Eagle's medium) supplemented with 2 mM l-glutamine, 100 U/mL penicillin, 100 μg/mL streptomycin, and 1 mg/mL gentamycin. To make the complete growth medium, 10 % (v/v) fetal bovine serum was added for skin fibroblast cells culture, and 10 % (v/v) equine serum was added for HeLa cells. Subculture was performed every 3-5 days for skin fibroblast cell lines, and every 2-3 days for HeLa cells at a ratio of 1:3-1:8. All cell lines were maintained at 37 ^{o}C, 5 % CO_2.

Cell viability and proliferation study. Cells were seeded in 6-well plates at the concentration of 1×10^5 cells/mL and were incubated for 48 h in standard culture medium at 37 °C in 5 % CO_2. After 48 hours, cells were incubated with a mixture of CNP-MSN and doxorubicin solution for 24 h. To compare with CNPs and MSN, we suspended CNPs or MSN in doxorubicin solution, and treated to cells for 24 h. As a control experiment, the cells were incubated with standard growth medium without adding any material for another 24 h. The cytotoxicity of this material with different cell lines was evaluated by Guava ViaCount cytometry assay (Guava Technologies, Inc.; Hayward, CA). Cell viability was calculated as the percentage of material treated cells to the untreated. While, cell proliferation was calculated as a percentage of the total cell amount treated with materials to that of control cell.

Endocytosis efficiency measurement. CNP-MSN was labeled by directly stirred with 1mg/ml FITC (fluorescein isothiocyanate) DMF solution for 2 h at room temperature. CNPs endocytosis study was measured by reacting with APTES (3-aminopropyltriethoxysilane) in toluene at 110 ^{o}C overnight firstly (mole ratio 1:1.5). After washed with methanol and dried in air, the afforded material was then stirred with 1mg/ml FITC DMF solution for 2 h. All the FITC labeled materials were washed extensively with methanol and dried in high vacuum at 100 ^{o}C to get rid of the organic solvent. Cells at a concentration of 1×10^{5} cells/mL were grown in 6-well plates for 48 h at 37 °C in 5 % CO_2. The cells were then treated with FITC-CNP-MSN and FITC-CNP which were suspended in serum-free media for 12 h at 37 °C in 5% CO_2. Then the cells were washed once with PBS and trypsinized. The cells were incubated in 830 mM trypan blue for 10 min to quench the fluorescence of any MSN nanoparticles adhered to the exterior of the cells. The cellular uptake was measured by flow cytometry.

Confocal fluorescence microscopy measurement. Skin fibroblast and HeLa cells were seeded at the density of 1×10^{5} cells per well in 6 well plates in 3 mL D-10 medium with coverslips at the bottom of the wells. For HeLa cells, after 36 h, the D-10 medium was replaced by 3 mL of material (10 μg/mL) in the serum-free DMEM medium for 10 h. For Skin fibroblast cells, after 60 h, the growth medium was changed by the material suspension medium. Afterwards, the medium was removed, the cells were washed with PBS (2×), and the cells were then reincubated with a PBS solution of 3.7 % formaldehyde and 57.0 mM 4,6-Diamidino-2-phenylindole dihydrochloride (DAPI) for 30 min. These coverslips were removed from the PBS solution and fixed to glass slides with liquid adhesive. The DAPI-stained coverslips were placed in microscope slides and examined under a Leica TCS NT

confocal fluorescence microscope system using a 100x oil immersion objective. As depicted in Figure 13 and 14, the blue fluorescent, DAPI-stained nuclei (right images) were observed by exciting the cells with a UV laser at wavelengths from 340 to 458 nm, while the green fluorescent FITC-CNP-MSN and FITC-CNP particles which inside cells were visualized by excitation at 488 nm with an Argon Laser. The phase contrast images of the cells were obtained with a 568 nm Krypton laser.

Instrumental method and characterization. X-ray diffraction patterns were collected from Rigaku ultima IV X-ray diffractometer using Cu Kα radiation. Nitrogen adsorption/desorption isotherm were measured by a Micromeritics Tristar 3000 sorptometer. The surface areas and pore size distributions were calculated by the Brunauer–Emmett–Teller (BET) and Barrett-Joyner-Halenda (BJH) method. The TEM examination was completed on a Tecnai G2 F20 and Philips CM 30 electron microscope operated at 200 kV. X-ray photoelectron spectroscopy were obtained from a Perkin-Elmer PHI 5500 XPS spectrometer with a hemispherical energy analyzer in an ion-pumped chamber (evacuated to 2×10^{-9} Torr), and a Al Kα (BE = 1486.6 eV) X-ray source at 250 W with 15 kV acceleration voltage. Peaks were assigned by using $Ce3d_{3/2}$ at 916 eV as charge compensation. The ζ - potential was measured in a Malvern Nano HT Zetasizer. Materials were dispersed with a concentration of 500 μg/ml in PBS buffer (pH 7.4, 10mM). Fluorescent intensity was obtained from FluoroMax-2. For fluorescein release, the excitation wavelength was at 480 nm and emission wavelength at 514 nm. For H_2DCF-DA on ROS measurement, the excitation wavelength was at 504 nm and emission wavelength at 524 nm. Thermogravimetric analysis was carried out on auto TGA 2950HR V5.7A thermal analyzer with a heating rate of 2˚C/min. Fourier transform infrared spectroscopy was measured by

Necolet Nexus 470 FTIR. ICP-MS was employed to determine the loading of cerium on MSN. The measurement was carried out on Agilent HP 4500. The calibration curve was prepared by measuring the standard solution with concentration from 20 ppm to 150 ppm. CNP-MSN 11.5 mg was dissolved in hydrofluoric acid (48 wt.%), and diluted to 100 ml. The loading of ceria on MSN is 92.2 μg/mg (Figure 19).

References

1. Lai, C. Y.; Trewyn, B. G.; Jeftinija, D. M.; Jeftinija, K.; Xu, S.; Jeftinija, S.; Lin, V. S. Y., *J. Am. Chem. Soc.* **2003,** *125* (15), 4451-4459.

2. Radu, D. R.; Lai, C. Y.; Jeftinija, K.; Rowe, E. W.; Jeftinija, S.; Lin, V. S. Y., *J. Am. Chem. Soc.* **2004,** *126* (41), 13216-13217.

3. Trewyn, B. G.; Whitman, C. M.; Lin, V. S. Y., *Nano Lett.* **2004,** *4* (11), 2139-2143.

4. Giri, S.; Trewyn, B. G.; Stellmaker, M. P.; Lin, V. S. Y., *Angewandte Chemie-International Edition* **2005,** *44* (32), 5038-5044.

5. Slowing, II; Trewyn, B. G.; Giri, S.; Lin, V. S. Y., *Adv. Funct. Mater.* **2007,** *17* (8), 1225-1236.

6. Slowing, II; Trewyn, B. G.; Lin, V. S. Y., *J. Am. Chem. Soc.* **2007,** *129* (28), 8845-8849.

7. Torney, F.; Trewyn, B. G.; Lin, V. S. Y.; Wang, K., *Nat. Nanotechnol.* **2007,** *2* (5), 295-300.

8. Trewyn, B. G.; Giri, S.; Slowing, II; Lin, V. S. Y., *Chemical Communications* **2007,** (31), 3236-3245.

9. Zhao, Y.; Trewyn, B. G.; Slowing, I. I.; Lin, V. S. Y., *J. Am. Chem. Soc.* **2009,** *131* (24), 8398-8400.

10. Mortera, R.; Vivero-Escoto, J.; Slowing, I. I.; Garrone, E.; Onida, B.; Lin, V. S. Y., *Chem. Commun. (Cambridge, U. K.)* **2009,** (22), 3219-3221.

11. Vivero-Escoto, J. L.; Slowing, I. I.; Wu, C.-W.; Lin, V. S. Y., *J. Am. Chem. Soc.* **2009,** *131* (10), 3462-3463.

12. Tarnuzzer, R. W.; Colon, J.; Patil, S.; Seal, S., *Nano Lett.* **2005,** *5* (12), 2573-2577.

13. Chen, J.; Patil, S.; Seal, S.; McGinnis, J. F., *Nat. Nanotechnol.* **2006,** *1* (2), 142-150.

14. Schubert, D.; Dargusch, R.; Raitano, J.; Chan, S.-W., *Biochem. Biophys. Res. Commun.* **2006,** *342* (1), 86-91.

15. Heckert, E. G.; Karakoti, A. S.; Seal, S.; Self, W. T., *Biomaterials* **2008,** *29* (18), 2705-2709.

16. Perez, J. M.; Asati, A.; Nath, S.; Kaittanis, C., *Small* **2008,** *4* (5), 552-556.

17. Karakoti, A. S.; Singh, S.; Kumar, A.; Malinska, M.; Kuchibhatla, S. V. N. T.; Wozniak, K.; Self, W. T.; Seal, S., *J. Am. Chem. Soc.* **2009,** *131* (40), 14144-14145.

18. Esch, F.; Fabris, S.; Zhou, L.; Montini, T.; Africh, C.; Fornasiero, P.; Comelli, G.; Rosei, R., *Science* **2005,** *309* (5735), 752-755.

19. Korsvik, C.; Patil, S.; Seal, S.; Self, W. T., *Chem. Commun. (Cambridge, U. K.)* **2007,** (10), 1056-1058.

20. Deshpande, S.; Patil, S.; Kuchibhatla, S. V. N. T.; Seal, S., *Appl. Phys. Lett.* **2005,** *87* (13), 133113/1-133113/3.

21. Park, E.-J.; Choi, J.; Park, Y.-K.; Park, K., *Toxicology* **2008,** *245* (1-2), 90-100.

22. Lin, W.; Huang, Y.-w.; Zhou, X.-D.; Ma, Y., *Int. J. Toxicol.* **2006,** *25* (6), 451-457.

23. Lin, V. S. Y.; Lai, C. Y.; Huang, J. G.; Song, S. A.; Xu, S., *J. Am. Chem. Soc.* **2001,** *123* (46), 11510-11511.

24. Lin, V. S. Y.; Radu, D. R.; Han, M. K.; Deng, W. H.; Kuroki, S.; Shanks, B. H.; Pruski, M., *J. Am. Chem. Soc.* **2002,** *124* (31), 9040-9041.

25. Chen, H.-I.; Chang, H.-Y., *Colloids Surf., A* **2004,** *242* (1-3), 61-69.

26. Sigler, P. B.; Masters, B. J., *J. Am. Chem. Soc.* **1957,** *79*, 6353-7.

27. Myers, C. E.; McGuire, W. P.; Liss, R. H.; Ifrim, I.; Grotzinger, K.; Young, R. C., *Science* **1977,** *197* (4299), 165-7.

28. Jung, K.; Reszka, R., *Adv. Drug Delivery Rev.* **2001,** *49* (1-2), 87-105.

29. Limbach, L. K.; Li, Y.; Grass, R. N.; Brunner, T. J.; Hintermann, M. A.; Muller, M.; Gunther, D.; Stark, W. J., *Environmental Science and Technology* **2005,** *39* (23), 9370-9376.

Tables and Figures

Table 1. Zeta potential, surface area, and pore volume of SH-MSN, linker-MSN, CNPs and CNP-MSN.

Materials	Zeta potential (mV)	BET surface area (m^2/g)	BJH pore volume (cm^3/g)
SH-MSN	-14.4	972	0.9
Linker-MSN	-2.33	918	0.8
CNPs	-43.1	-	-
CNP-MSN	-5.49	325	< 0.2

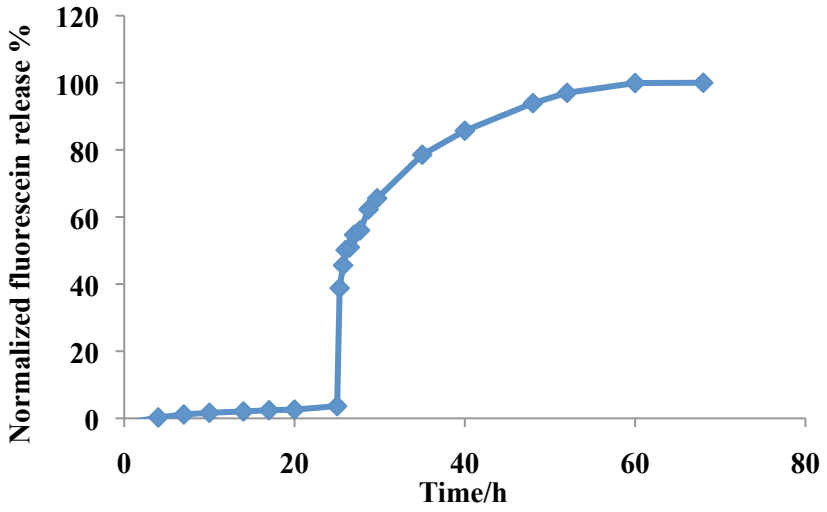

(a)

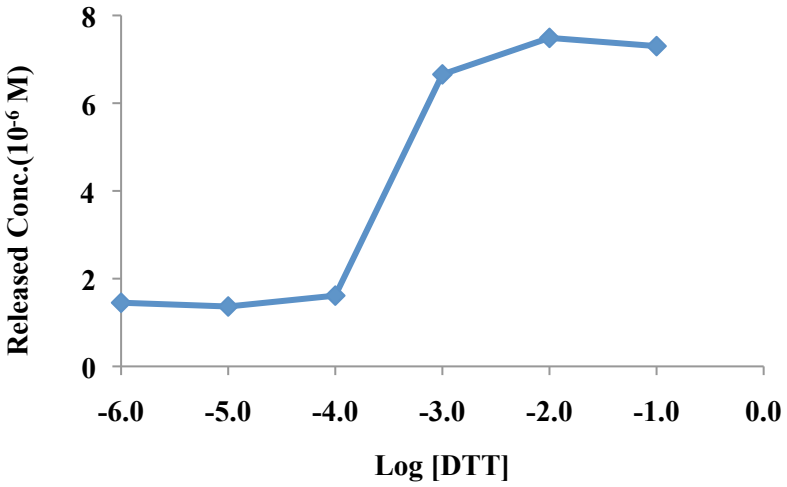

(b)

Figure 1. DTT induced controlled release curve of fluorescein loaded, TESSA-CNP capped MSN (a); total released fluorescein concentration vs. DTT concentration (b).

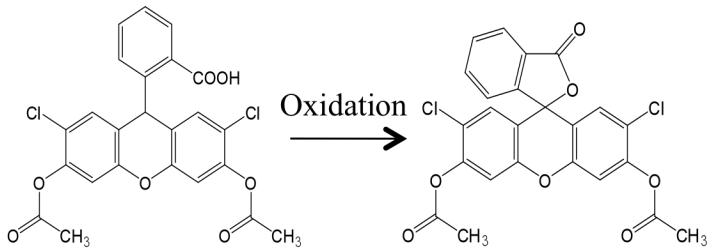

H_2DCF-DA DCF-DA

Figure 2. 2',7'-dichlorofluorescein diacetate (H_2DCF-DA) is oxidized to highly fluorescent DCF-DA by H_2O_2.

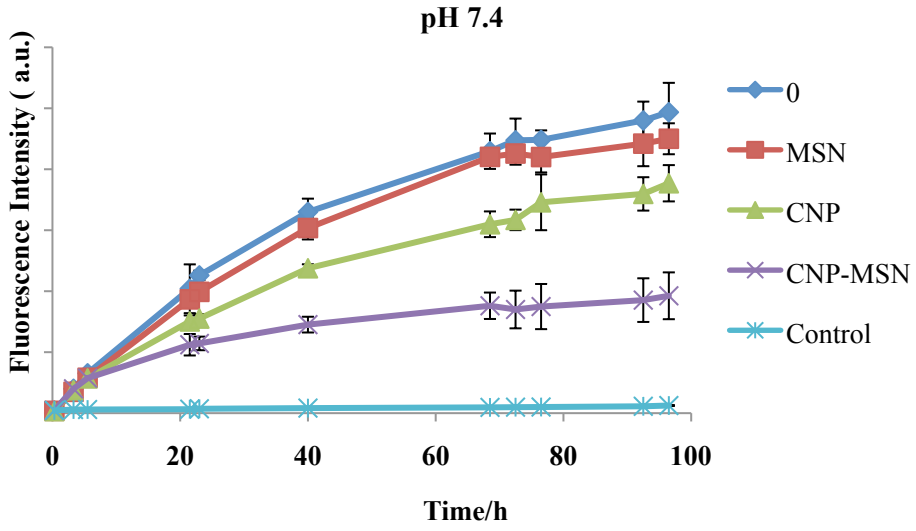

(a)

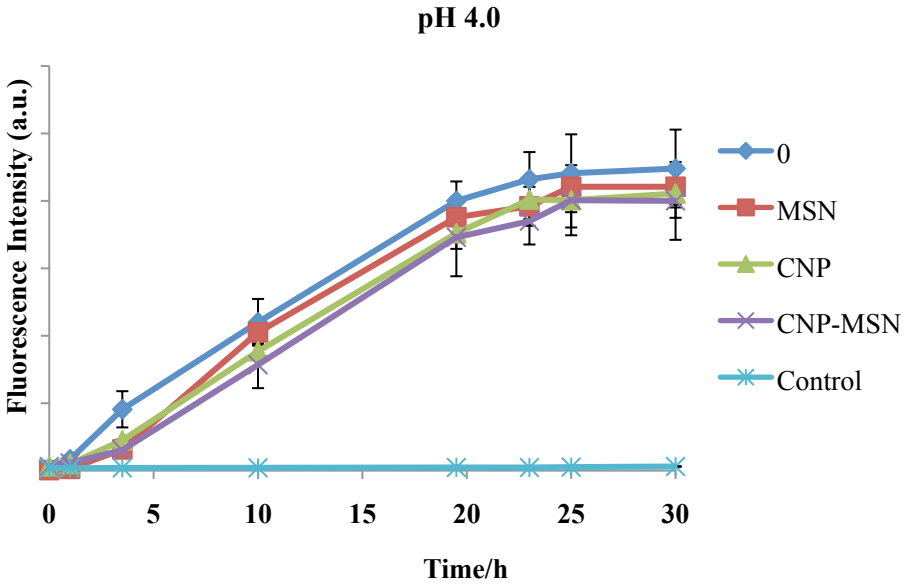

(b)

Figure 3. Fluorescence intensity curve vs. time at pH 7.4 (a) and pH 4 (b). Positive control is denoted as 0, whereas negative control is labeled as Control.

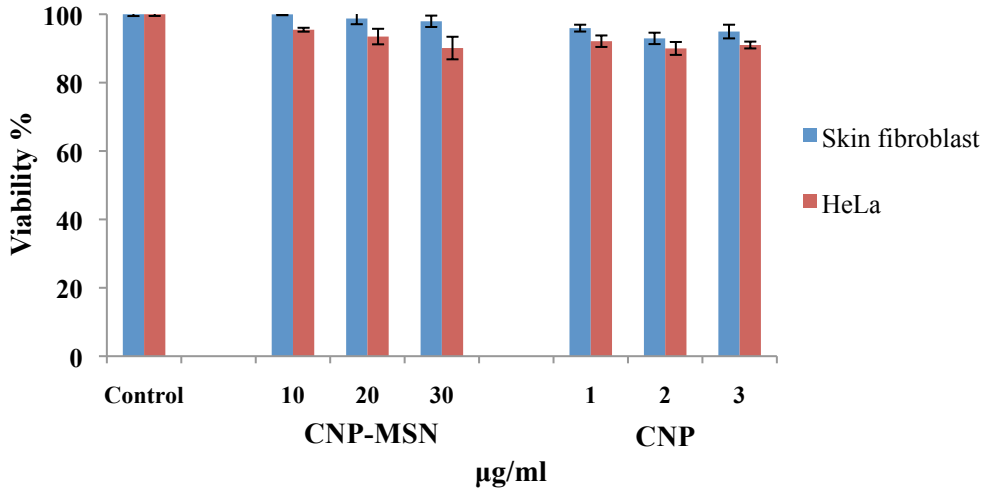

Figure 4. Viability and proliferation of skin fibroblast cell and HeLa cell under the treatment of CNP-MSN and CNPs with different concentrations for 24h.

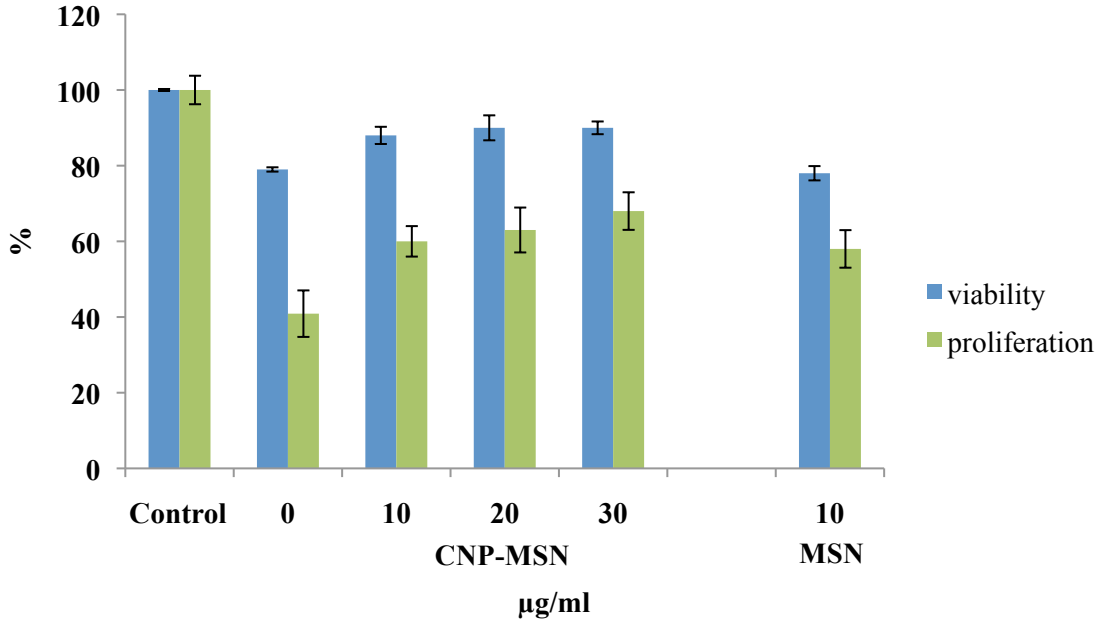

Figure 5. Viability and proliferation of skin fibroblast cells after treated with the mixture of CNP-MSN and 2 µM doxorubicin for 24 h. MSN was used as comparison.

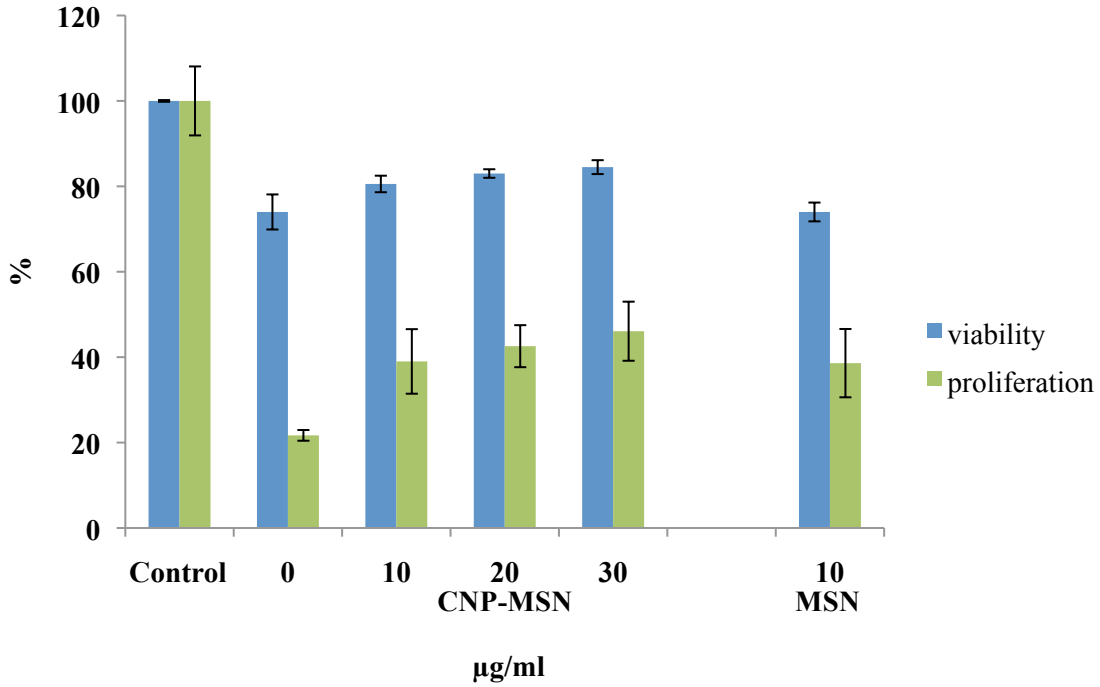

Figure 6. Viability and proliferation of skin fibroblast cells after treated with the mixture of CNP-MSN and 5 µM doxorubicin for 24h. MSN was used as comparison.

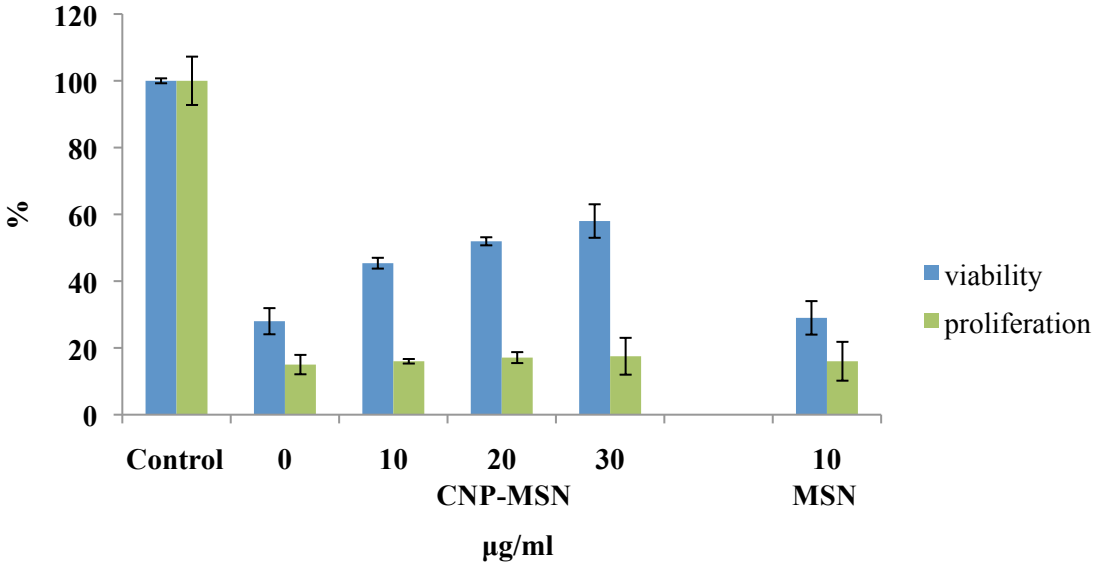

(a)

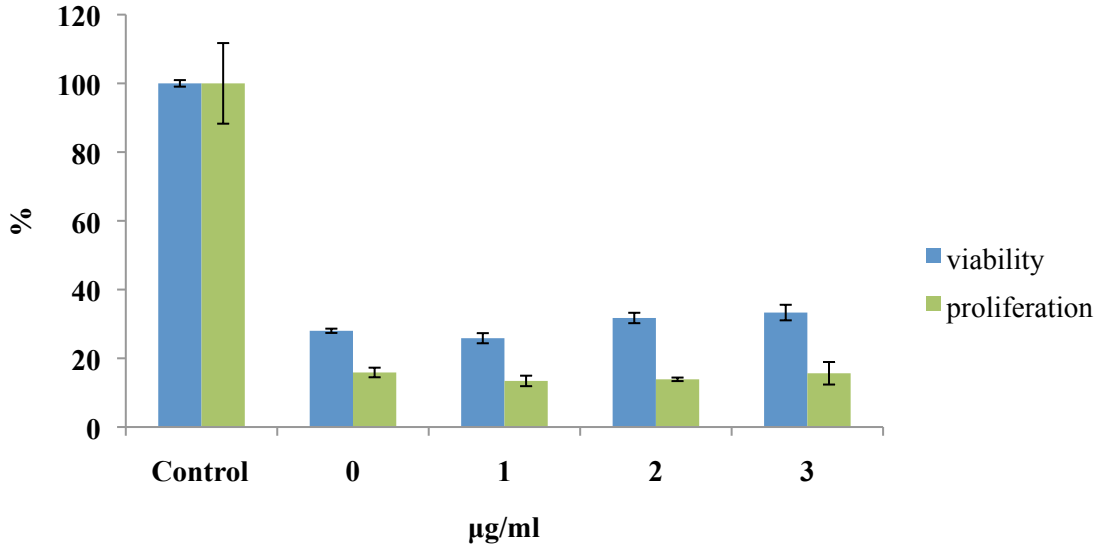

(b)

Figure 7. Viability and proliferation of skin fibroblast cells after treated with the mixture of 10 µM doxorubicin and CNP-MSN (a) and CNPs (b) for 24h.

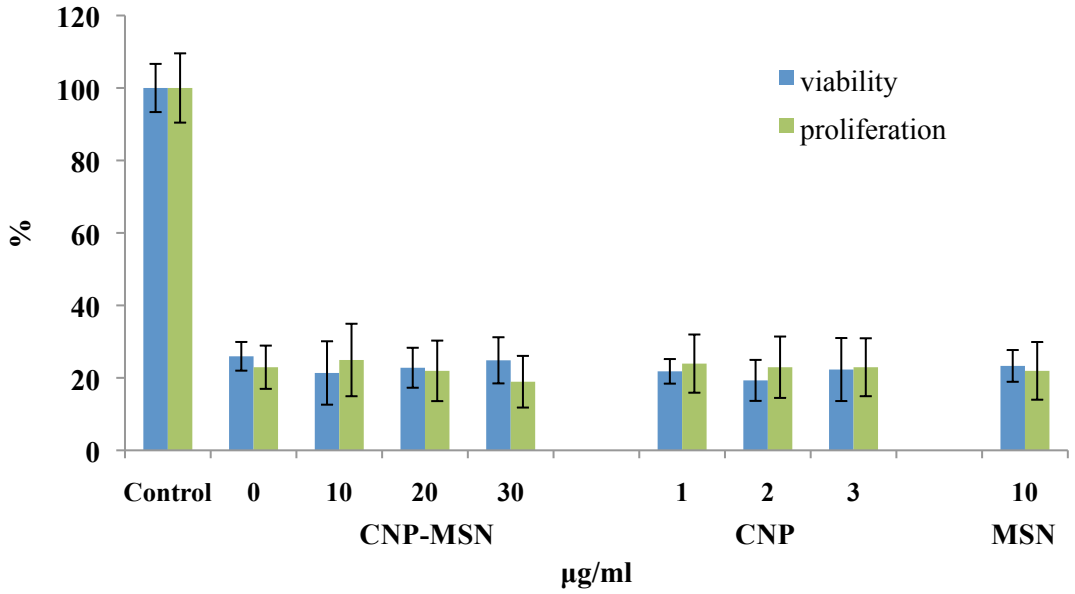

Figure 8. Viability and proliferation of HeLa cells after treated with the mixture of 10 µM doxorubicin with CNP-MSN and CNPs for 24h.

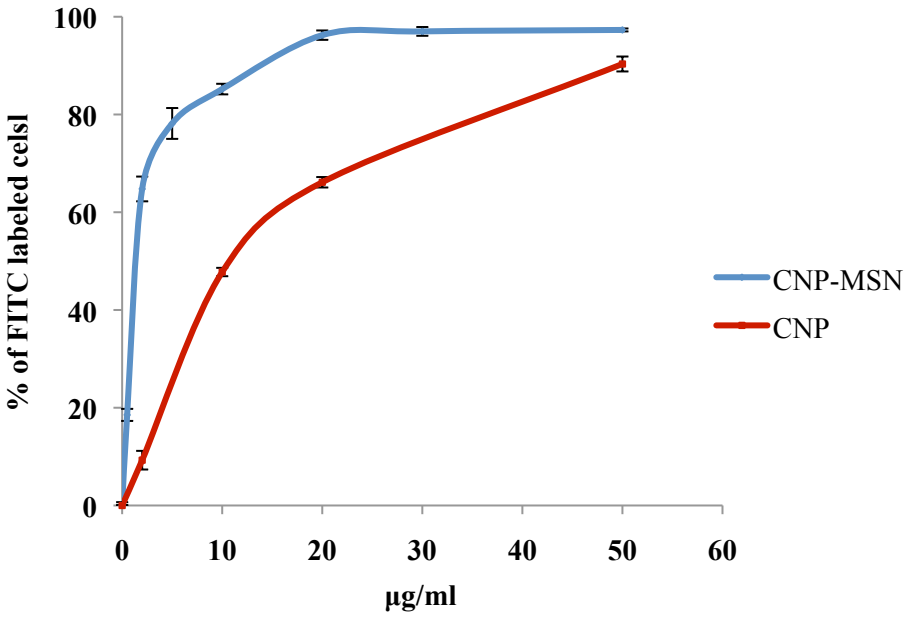

Figure 9. Endocytosis efficiency of CNP-MSN and CNPs under different concentrations by skin fibroblast cells.

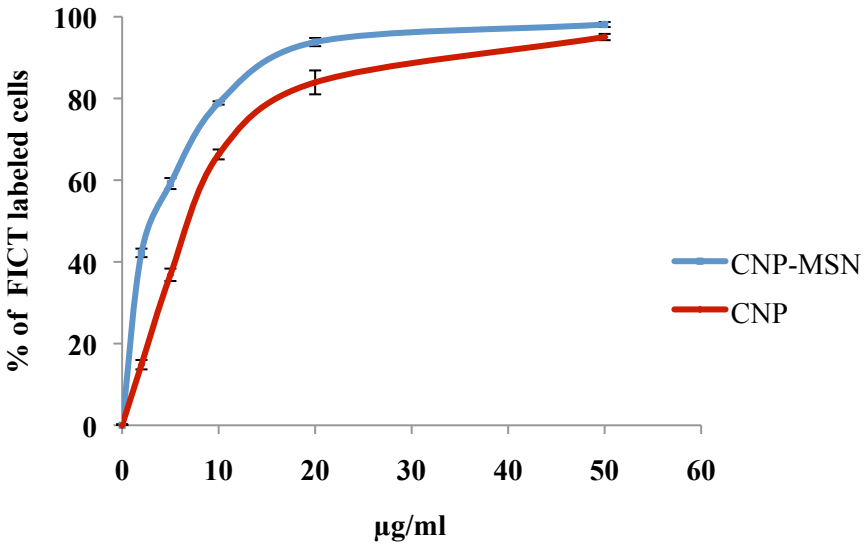

Figure 10. Endocytosis efficiency of CNP-MSN and CNPs under different concentrations by HeLa cells.

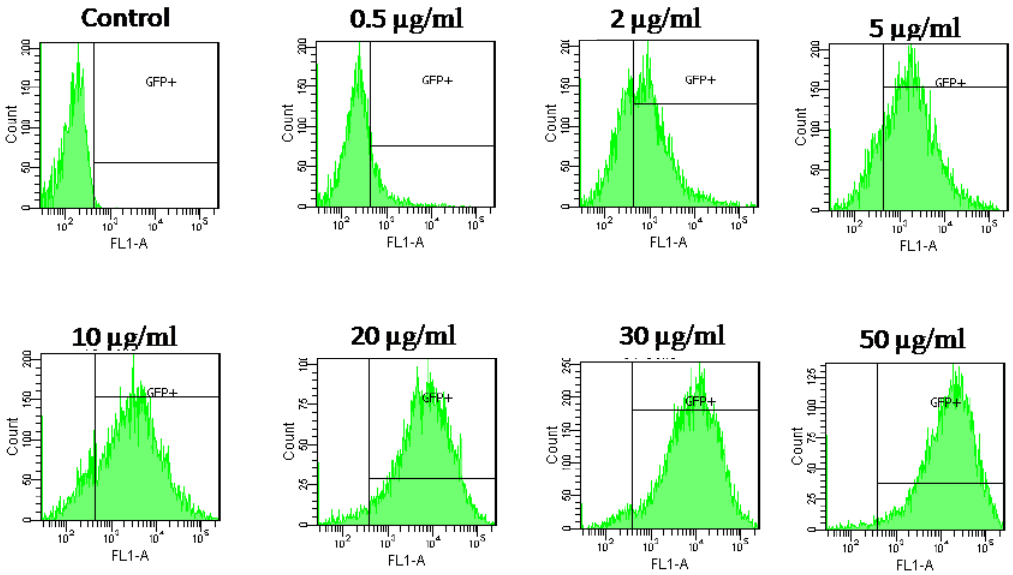

(a)

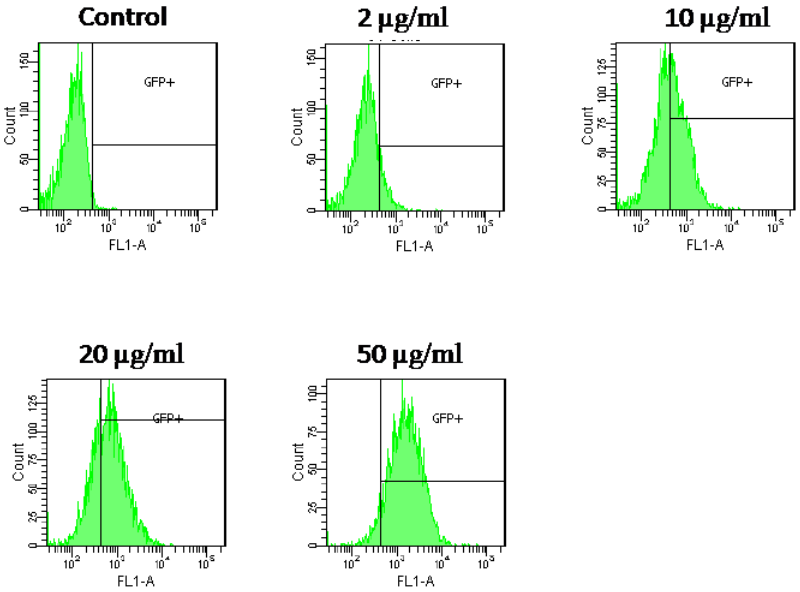

(b)

Figure 11. Fluorescence histograms of skin fibroblast cells after treated with FITC-labeled materials (a) CNP-MSN, EC_{50} ~1.5 µg/ml; (b) CNP, EC_{50} ~10 µg/ml. Representative results of three independent experiments.

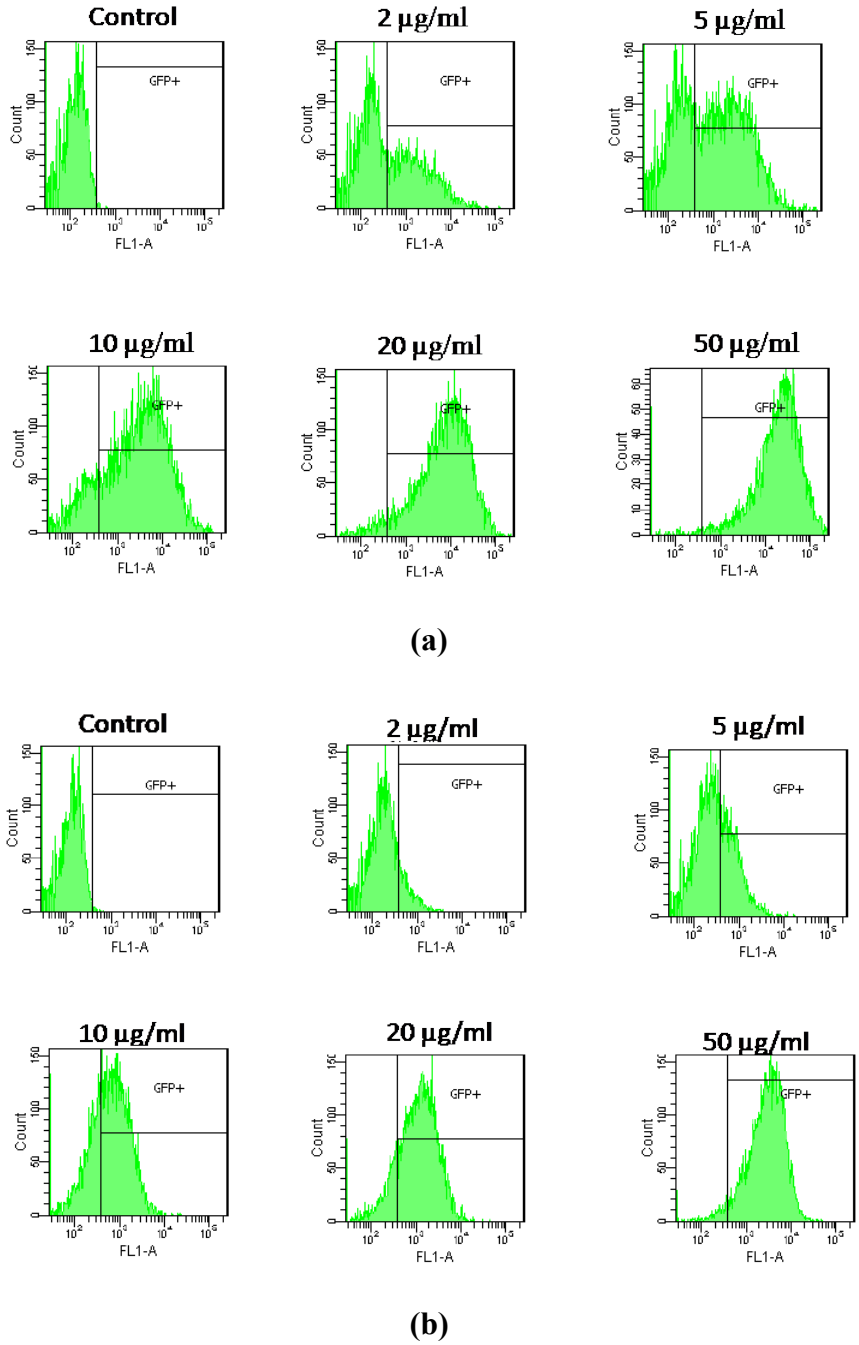

Figure 12. Fluorescence histograms of HeLa cells after treated with FITC-labeled materials (a) CNP-MSN, EC_{50} ~ 4 µg/ml; (b) CNP, EC_{50} ~ 8 µg/ml. Representative results of three independent experiments.

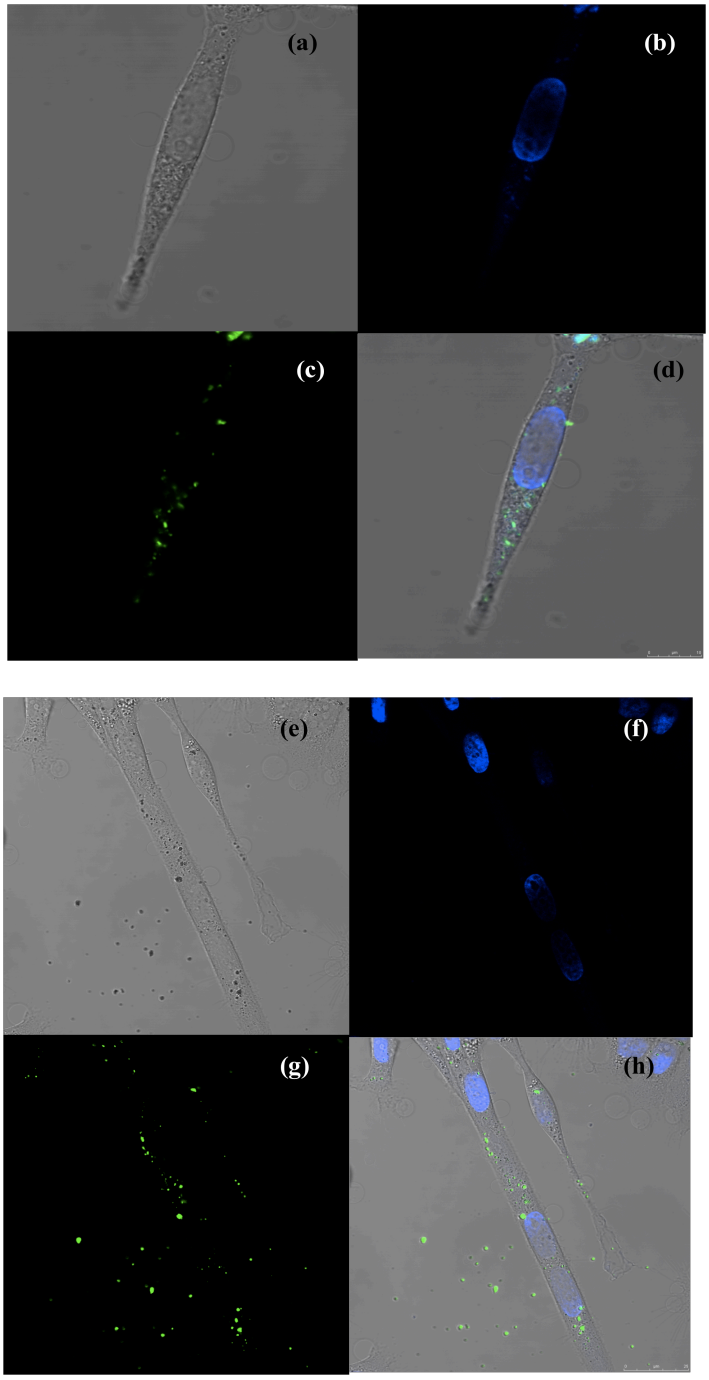

Figure 13. Fluorescence confocal micrographs of skin fibroblast cells internalized with 10 µg/ml FICT labeled (green) CNP-MSN (c), CNP (g); Stained with nuclei dye DAPI (blue) (b) and (f); (a) and (e) are Differential Interference Contrast (DIC) micrograph. The merged micrograph are shown in (d) and (h).

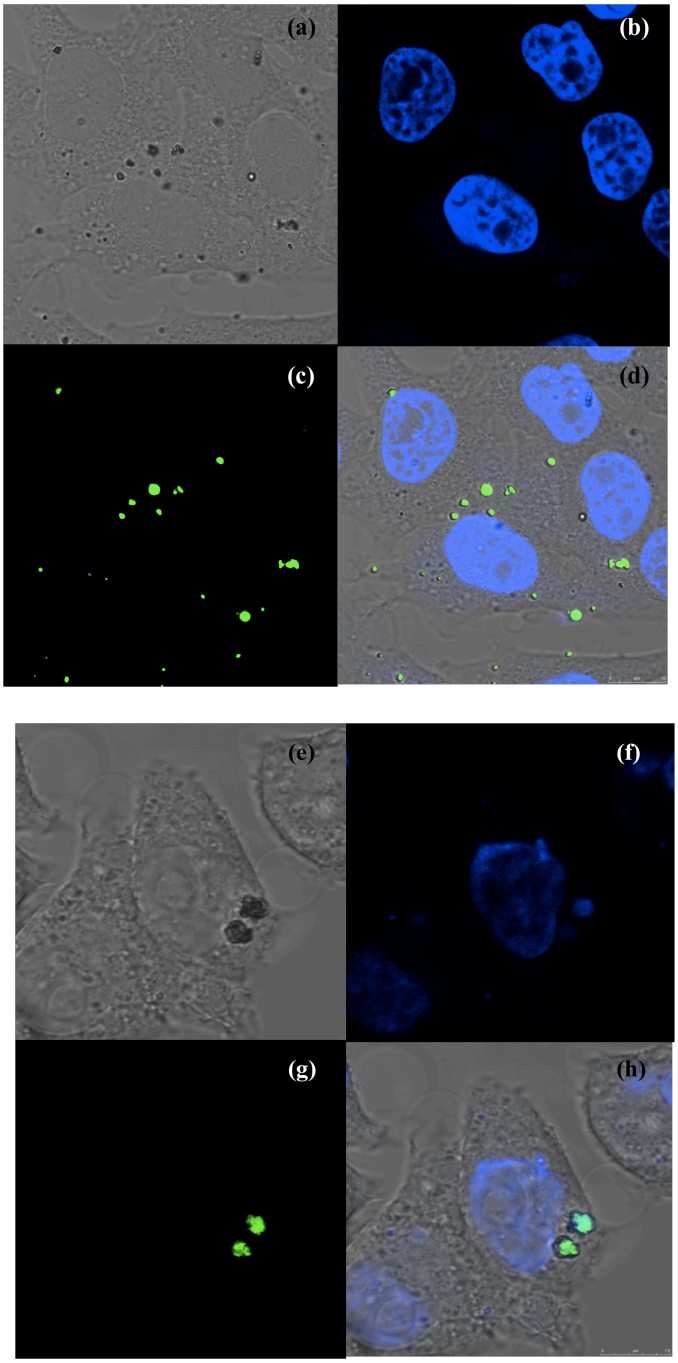

Figure 14. Fluorescence confocal micrographs of HeLa cells internalized with 10 µg/ml FICT labeled (green) CNP-MSN (c), CNP (g); Stained with nuclei dye DAPI (blue) (b) and (f); (a) and (e) are Differential Interference Contrast (DIC) micrograph. The merged micrograph are shown in (d) and (h).

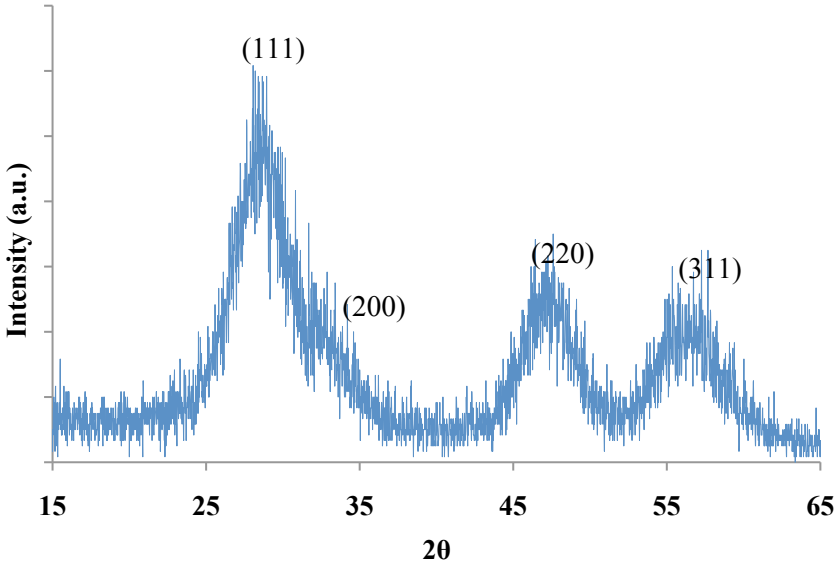

(a)

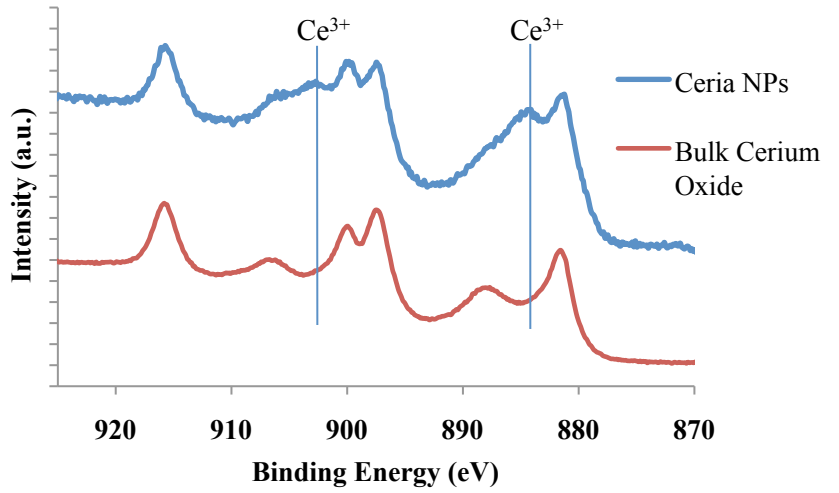

(b)

Figure 15. X-ray diffraction of CNP (a); X-ray photoelectron spectroscopy of CNP vs. bulk cerium oxide (b).

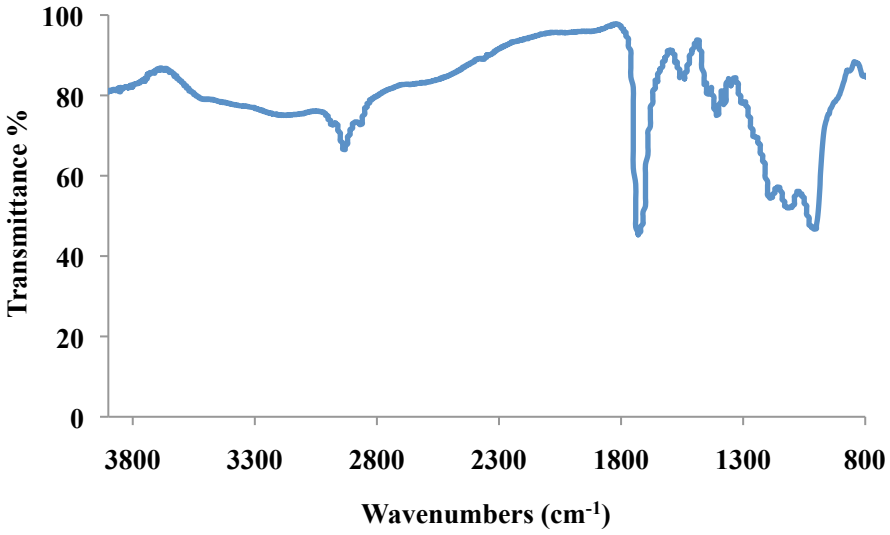

Figure 16. Fourier transform Infrared Spectroscopy of TESSA grafted CNP.

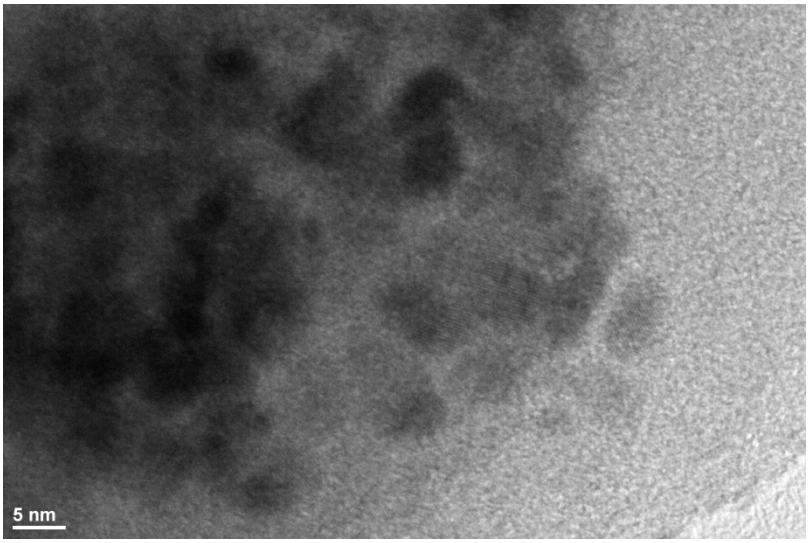

(a)

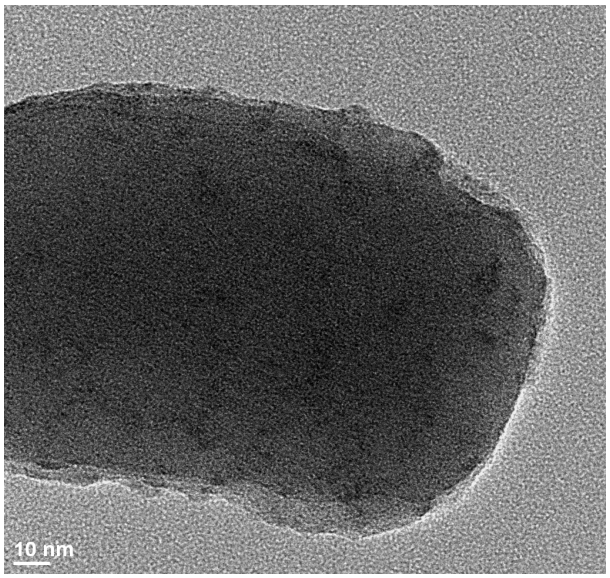

(b)

Figure 17. Transmission electron microscopy of (a) CNPs; (b) CNP-MSN.

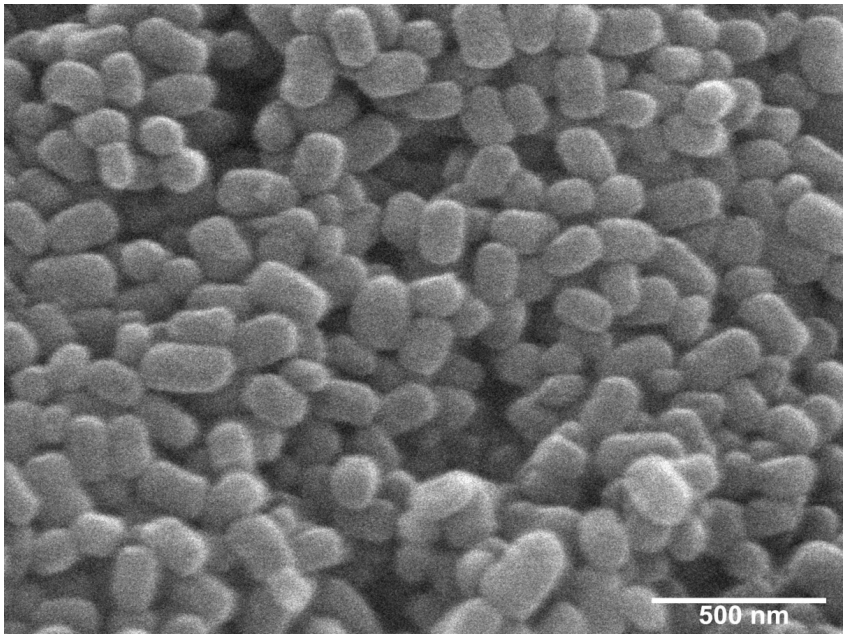

Figure 18. Scanning electron microscopy of linker-MSN

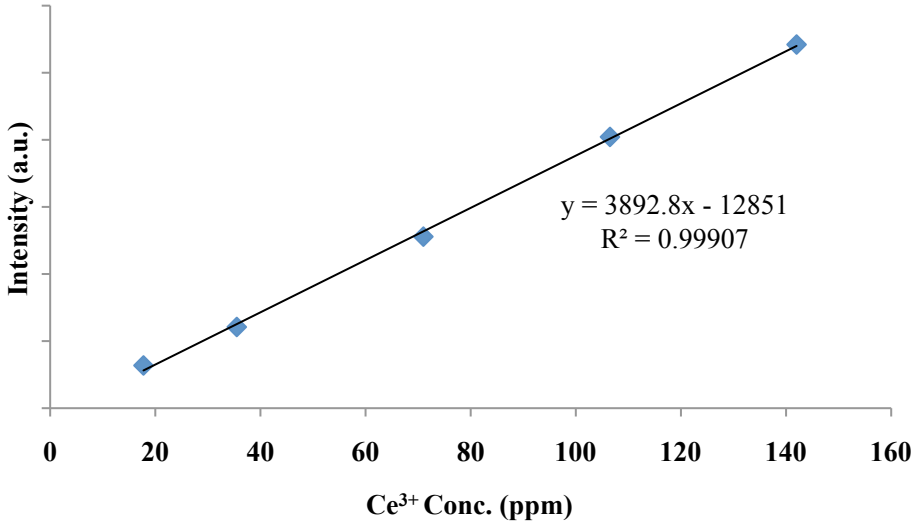

Figure 19. ICP-MS calibration curve of Ce^{3+} concentration vs. intensity.

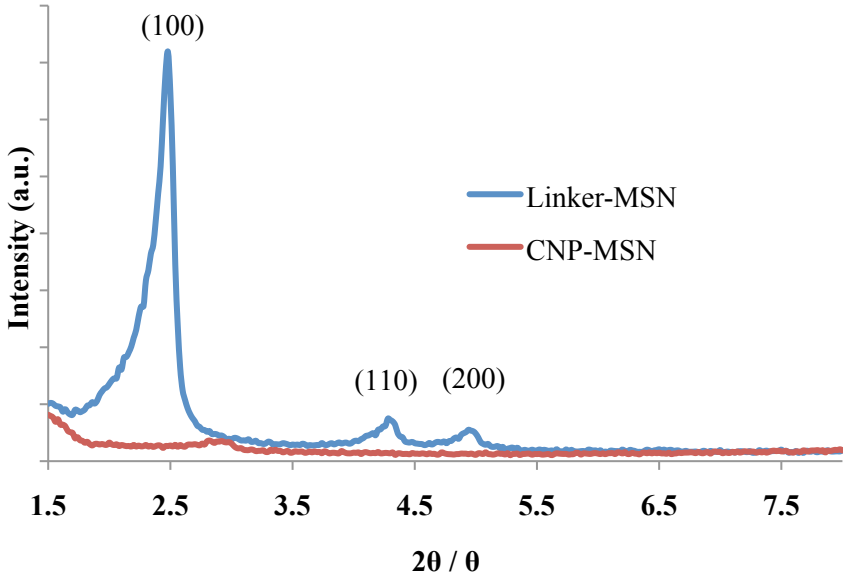

Figure 20. X-ray diffraction of linker-MSN and CNP-MSN.

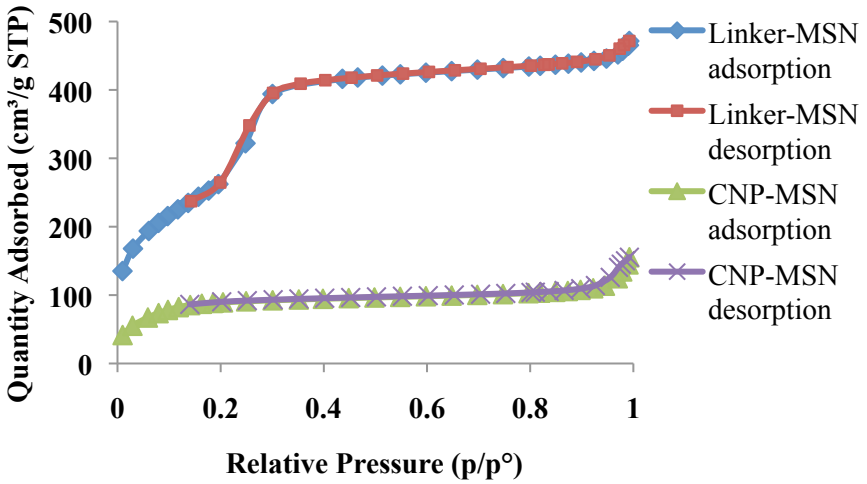

(a)

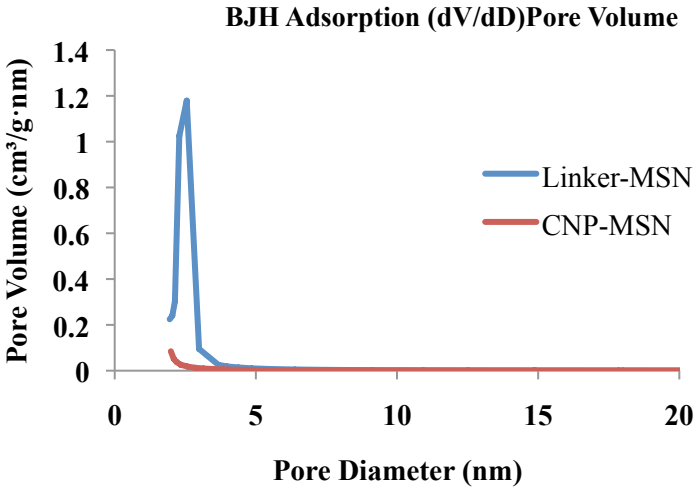

(b)

Figure 21. Nitrogen ad/desorption isotherm of linker-MSN and CNP-MSN by Brunauer–Emmett–Teller (BET) method (a) and pore size distribution by Barrett-Joyner-Halenda (BJH) method (b).

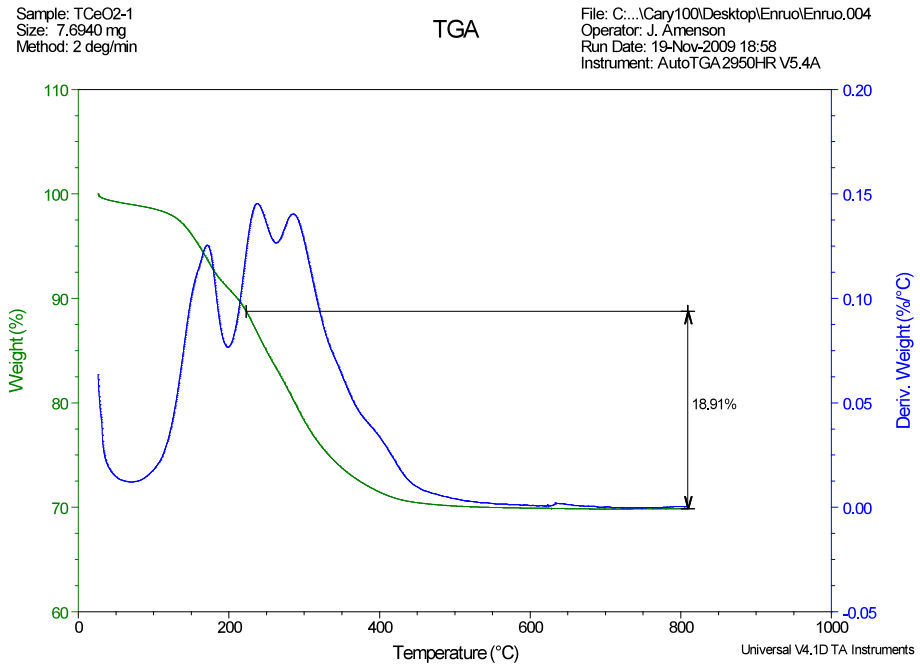

(a)

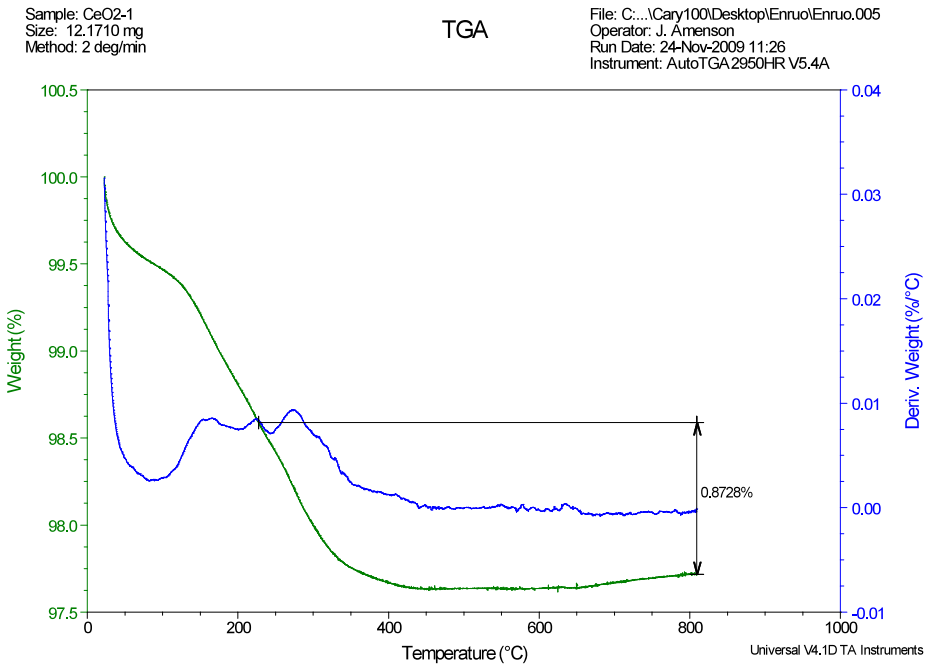

(b)

Figure 22. Weight loss of TESSA-CNP (a) and CNP (b) by TGA.

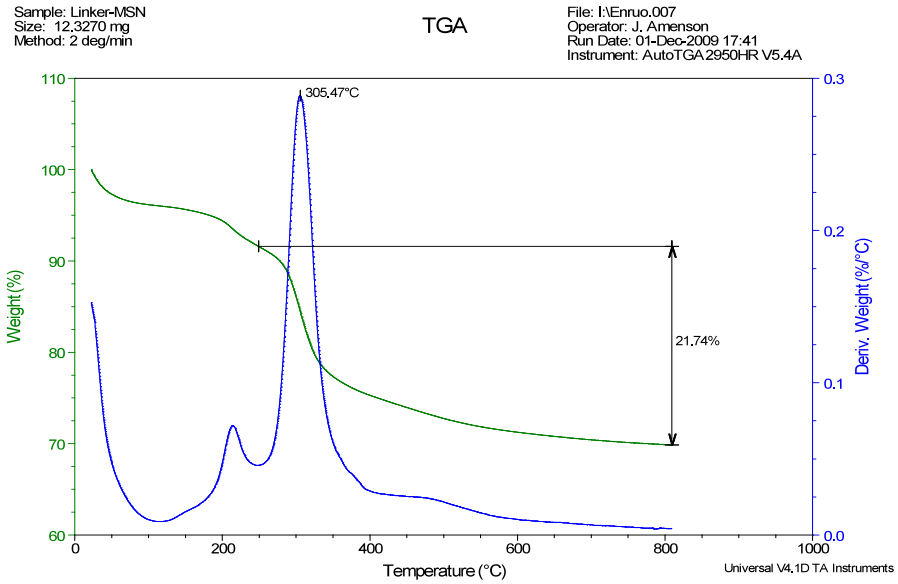

(a)

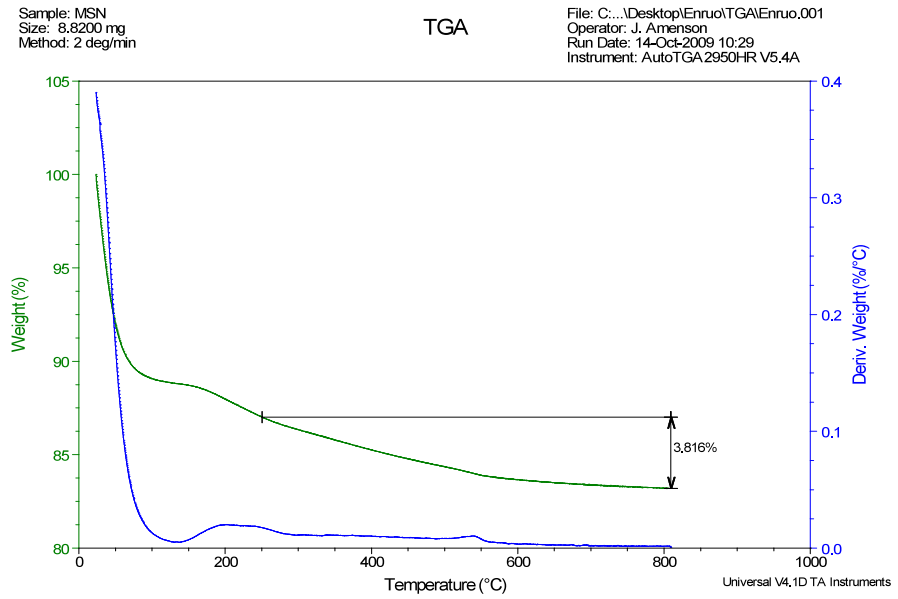

(b)

Figure 23. Weight loss of Linker-MSN (a) and blank MSN (b) by TGA.

CHAPTER 5. GENERAL CONCLUSIONS

Mesoporous silica nanoparticles (MSN) have been extensively studied due to its unique characteristics, such as high surface area, ordered pore structure, large pore volume, tunable pore size and biocompatibility. With the efforts in Dr. Victor Lin's group, these applications were involved in supports for noble metal particles in catalysis, vehicles for controlled release and intracellular drug delivery.

The synthesis of ethanol selectively from syngas (CO and H_2), which can be made from coal or biomass pyrolysis, has been a topic of growing interests from both industrial and academic points of views. Among many candidates, Rhodium based catalysts have been known for decades for an excellent selectivity in C_{2+} oxygenates, including ethanol, due to the unique CO adsorption behavior on Rh surface. However, the size control of Rh particles and migration and growth in high temperature process, problematically decrease the reactivity in a large degree. In our study, we successfully synthesized well-defined Rh particles with 2 nm size in alcoholic solution using polyvinylpyrrolidone (PVP), as a nanoparticle stabilizer, and subsequent encapsulated the as-made Rh nanoparticles in the framework of MSN during *in situ* precipitation. After further modified by manganese oxide, the material showed much higher selectivity as well as conversion comparing to the commercial Rhodium based catalysts. Even though the *in situ* encapsulation methods has been reported recently, there are still a large potential to study, such as a more sophisticated synthetic way, loading of new metallic or metal oxide nanoparticles in the application of other catalytic process.

We synthesized a series of mesoporous calcium silicate materials by applying an anionic surfactant (PME) as the structure directing agent. In our study, positively charged calcium ions were introduced to interact with the phosphate groups of the anionic PME surfactant molecules. Under basic conditions, hydrolyzed TEOS easily coordinates with the calcium/surfactant in a $S^-M^+I^-$ complex system and forms ordered structure. After the removal of surfactants, the calcium sites would be exposed to the surface and be accessible to the reactants. By adjusting the synthetic parameters, such as two inorganic precursors mole ratio, concentration, pH, we successfully made the highly reactive catalysts for transesterification reaction from soybean oil to biodiesel. The best catalyst can achieve a quantitative yield in less than two hours, which is quite competitive to the commercially used homogenous catalysts. Furthermore, the catalysts can be recycled several times. The strategy of using anionic surfactant to template mesoporous calcium silicate is a brand new method in heterogeneous catalysts for biodiesel production, which would even further a new generation of catalysts.

The controlled-release of "hard-cap" facilitated system is also investigated. Ceria nanoparticles (CNPs) have attracted many attentions in the biomedical field recently, due to the redox chemistry on its surface. We studied CNPs as antioxidant as well as the mesopore caps to scavenge reactive oxygen species. The functionalized MSN with disulfanyl ethylamine group can covalently linked with succinic acid grafted ceria nanoparticles. While the disulfide bond can be cleaved by disulfide reducing agent (DTT), which regulates the removing of ceria caps. It shows a good controlled release system. Also, the system performed pH-dependent antioxidant property when exposed to H_2O_2, and even showed to suppress ROS more efficiently than naked CNPs. After comparing the endocytosis

efficiency, we found MSN could facilitate and help the uptake of CNPs by skin fibroblast cells. CNP-MSN showed nearly ten times higher efficiency than naked CNPs. We suspected the porous structure of MSN played a big role in the process, whereas the mechanism is still under investigation. The antioxidant and free radical scavenging property of CNPs would obtain further interest, which is related to functionalization and targeting.

In addition to the applications of MSN we discussed above, there are other applications which have been or will be studied in the next few years, such as absorbents, sensors, templates and molecular sieves. All these applications are associated with functionalization on the surface, tuning the pore size and morphology control.